Groundwater controls on post-fire permafrost thaw: Water and energy balance effects

Samuel C. Zipper[1,2], Pierrick Lamontagne-Hallé[1], Jeffrey M. McKenzie[1], Adrian V. Rocha[3]

[1]Department of Earth and Planetary Sciences, McGill University, Montreal QC, Canada

[2]Department of Civil Engineering, University of Victoria, Victoria BC, Canada

[3]Department of Biological Sciences and the Global Change Initiative, University of Notre Dame, Notre Dame IN, USA

Corresponding author: Samuel C. Zipper (samuelczipper@gmail.com)

Key Points:

- Ignoring groundwater flow may cause over/underestimation of the influence of thermal/hydrologic properties on post-fire permafrost thaw
- Post-fire increases in soil temperature increase both conductive and advective heat transport, leading to a thicker active layer
- Lateral thaw depth variability and groundwater discharge to streams decrease following fire due to decreased groundwater recharge

Abstract

Fire frequency and severity are increasing in high latitude regions, but the degree to which groundwater flow impacts the response of permafrost to fire remains poorly understood. Here, we use the Anaktuvuk River Fire (Alaska, USA) as an example for simulating groundwater-permafrost interactions following fire. We identify key thermal and hydrologic parameters controlling permafrost response to fire both with and without groundwater flow, and separate the relative influence of changes to the water and energy balances on active layer thickness. Our results show that mineral soil porosity, which influences the bulk subsurface thermal conductivity, is a key parameter controlling active layer response to fire in both the absence and presence of groundwater flow. However, neglecting groundwater flow increases the perceived importance of subsurface thermal properties, such as the thermal conductivity of soil solids, and decreases the perceived importance of hydrologic properties, such as the soil permeability. Furthermore, we demonstrate that changes to the energy balance (increased soil temperature) drive increased active layer thickness following fire, while changes to the water balance (decreased groundwater recharge) lead to reduced landscape-scale variability in active layer thickness and groundwater discharge to surface water features such as streams. These results indicate that explicit consideration of groundwater flow is critical to understanding how permafrost environments respond to fire.

Plain Language Summary

While scientists know permafrost (areas of permanently frozen ground) often thaws following fire, it is not well understood if groundwater movement enhances or reduces this thawing process. In this study, we simulate the response of permafrost to fire using models that both include and ignore groundwater flow with many different model input datasets. Our results show that when groundwater flow is ignored, the relative importance of soil properties associated with heat movement may be overestimated, and the importance of soil properties associated with water movement are likely to be underestimated. Additionally, we show that increased soil temperature is the most important factor leading to deeper permafrost thaw following fire. However, lower groundwater recharge rates at burned locations decreased permafrost thaw differences between upland and lowland regions of a watershed, as well as groundwater flow into streams and rivers.

Index Terms:

1829 Groundwater hydrology; 0475 Permafrost, cryosphere, and high-latitude processes; 0764 Energy balance; 1655 Water cycles; 1846 Model calibration

Keywords:

tundra fire; Long-Term Ecological Research (LTER) network; active layer thickness; baseflow; Arctic; groundwater modeling;

1 Introduction

Fire frequency and severity in the Arctic are expected to increase in the future and can have large-scale and long-lasting effects on hydrological and biogeochemical cycling (Flannigan et al., 2005; Hu et al., 2015). For instance, fire can change the landscape locally by enhancing erosion and thermokarst development (Chipman & Hu, 2017; Iwahana et al., 2016; Jones et al., 2015), and can have global impacts by releasing soil carbon that contributes to global climate change (Abbott et al., 2016; Balshi et al., 2007; Schuur et al., 2015). In continuous permafrost settings, these changes are primarily driven by increases in the thickness of the active layer (the soil above the permafrost which thaws and refreezes annually) following fire. Therefore, understanding the processes underlying post-fire active layer dynamics is essential to anticipate and mitigate changes to the Arctic landscape as well as to understand fire impacts on global carbon cycling.

Increases in active layer thickness following fire occur via two mechanisms: (1) thinning the near-surface organic soil layer which acts as a thermal buffer between air and the subsurface (Brown et al., 2015, 2016; Kasischke & Johnstone, 2005), and (2) decreasing albedo which increases energy input into the subsurface (Rocha & Shaver, 2011b; Smith et al., 2015; Yoshikawa et al., 2002). Past modeling efforts studying post-fire active layer thickness have primarily concluded that soil thermal properties are the most important control on permafrost response to fire (Jiang et al., 2012, 2015b; Yi et al., 2009). However, these studies neglected the potential impacts of lateral groundwater flow on permafrost thaw by using one-dimensional models (Brown et al., 2015; Jiang et al., 2015b; Treat et al., 2013; Yi et al., 2009; Zhang et al., 2003, 2015; Zhuang et al., 2002).

In contrast, however, field research shows that drainage patterns and soil texture influence permafrost response to fire (Kasischke et al., 2007; Minsley et al., 2016), implying that groundwater fluxes may be an important control on post-fire permafrost thaw. Increased subsurface hydrological connectivity, which is associated with thickening active layers, has been shown to lead to positive feedbacks on permafrost thaw by increasing advective heat transport via groundwater flow (Bense et al., 2009, 2012; Connon et al., 2014; Kurylyk et al., 2016; Lamontagne-Hallé et al., 2018; McKenzie & Voss, 2013; Walvoord et al., 2012), although this has not been studied in the context of fire. Similar processes could result in a positive post-fire feedback on permafrost degradation. However, the influence of groundwater flow on post-fire changes in active layer thickness is not well understood due to a lack of available data in high-latitude regions. Furthermore, no previous modelling work has investigated the importance of fire-induced feedbacks between groundwater flow and permafrost degradation. Understanding interactions between groundwater flow and permafrost dynamics is key to predicting and planning for future change in the water and energy balances of cold regions, particularly since fire effects will be superimposed on a warming trend which is already contributing to permafrost thaw across the Arctic (Hu et al., 2015; Lique et al., 2016; Walvoord & Kurylyk, 2016; Wrona et al., 2016).

To address this knowledge gap, this study explores the question, *how does groundwater flow impact permafrost response to fire?* We use an archetypal modeling approach, where a real-world domain is simplified to isolate specific processes (Zipper et al., 2018), to answer this research question. Our models are driven by field observations from three sites along a burn severity gradient (i.e. severe, moderate, and unburned) following the 2007 Anaktuvuk River Fire (ARF), which was the largest recorded tundra fire in history (Mack et al., 2011). The sites exhibited a large gradient in soil thermal dynamics that allowed us to address three specific sub-questions: (i) what is the relative importance of subsurface thermal and hydrologic properties in governing post-fire active layer thickness?; (ii) how does the importance of these properties change in the presence or absence of groundwater flow?; and (iii) how do post-fire changes to the water and energy balances interact to influence active layer thickness and groundwater discharge to streams?

While previous work (cited above) has suggested that thermal properties (conductivity and specific heat) are the key control on active layer thickness, we hypothesize that the importance of thermal properties is overestimated in previous modeling studies due to a lack of advective heat transport through groundwater flow. Therefore, when groundwater flow is considered, the relative importance of hydrologic properties (soil permeability and porosity) as a control over active layer thickness will likely increase. Furthermore, we hypothesize that changes to the energy and water balances following fire will have opposing effects, with increases in soil temperature leading to increased active layer thickness via enhanced heat conduction into the subsurface, but counteracted by decreases in groundwater recharge that reduce advective heat transport via groundwater flow.

2 Methodology

2.1 Anaktuvuk River Fire

The ARF burned ~1000 km^2 of Alaska's North Slope from July through October of 2007 (Jones et al., 2009). The ARF is thought to be an analog for a future Arctic in which warmer temperatures and expanding shrub extent lead to more large fires, though future climate impacts on Arctic fire regimes are highly uncertain (Higuera et al., 2008; Hu et al., 2010, 2015). Additionally, the severity of the fire varied over the large area burned, providing a gradient of burn severity which can be used to relate the ARF to fires of varying magnitudes elsewhere. Finally, the ARF has been studied in detail due to its proximity to the Toolik Lake Long-Term Ecological Research (LTER) field station, providing a rich interdisciplinary body of knowledge to contextualize our study (Bret-Harte et al., 2013; De Baets et al., 2016; Jiang et al., 2015a, 2017; Mack et al., 2011; Neilson et al., 2018; Rocha & Shaver, 2011a).

In the present study, we use three sites across a burn severity gradient which were instrumented with eddy covariance towers in June 2008, which we will refer to as Unburned (UB; 68.99°N, 150.28°W), Moderate Burn (MB; 68.95°N, 150.21°W), and Severe Burn (SB;

68.93°N, 150.27°W). The UB site is tundra tussock which was not affected by the fire; the MB site is a mix of partially and completely burned areas; and all vegetation was burned at the SB site (Rocha & Shaver, 2009, 2011a). Following the ARF, a decrease in soil organic layer thickness and albedo led to higher summer soil temperature at the MB and SB sites relative to the UB baseline; and evapotranspiration increased due to surface ponding following the loss of soil organic matter (Jiang et al., 2015b; Rocha & Shaver, 2011b).

2.2 Modeling approach

To test our hypotheses, we used a suite of numerical model simulations that are representative of the ARF sites. We use the modified version of the SUTRA numerical model (Voss & Provost, 2010) described in McKenzie et al. (2007) and McKenzie & Voss (2013). The modified model simulates saturated groundwater flow including freeze/thaw processes, which impact subsurface hydrologic and thermal properties based on the relative composition of three materials: liquid water, solid water (ice), and matrix material (soil solids). While there are various approaches to coupled simulations of groundwater and heat transport in freeze/thaw settings, the InterFrost model comparison project found that this modified version of SUTRA performed comparably to other codes including freeze-thaw processes (Grenier et al., 2018).

Our guiding principle in model design was that of parsimonious archetypal modeling, or making a groundwater flow model in "the simplest way possible that captures the most important overall behavior" (Voss, 2011b, p. 1456). Thus, rather than building a highly parameterized site-specific calibrated model, we made several simplifying assumptions to isolate the aspects of the domain most relevant to our research questions (Zipper et al., 2018). At a high level, we simplified the landscape to a two-dimensional cross-section with a fully saturated subsurface, which is commonly assumed when modeling groundwater-permafrost interactions (Ge et al., 2011; Kurylyk et al., 2016; McKenzie et al., 2007; McKenzie & Voss, 2013; Wellman et al., 2013). Specific assumptions related to the domain, boundary conditions, and model inputs are described in the sections below, and we discuss the potential implications of these assumptions in Section 4.4.

In our model, permeability is defined for the solid matrix material, and reduced as a function of liquid pore-water saturation using a relative permeability scaling coefficient. This coefficient is multiplied by the solid matrix permeability to obtain the effective permeability. We simulated saturated groundwater flow only, meaning that liquid pore-water saturation decreases when ice forms due to pore-water freezing, though the water table is not prescribed at the top of our domain and therefore hydraulic gradients may vary (Section 2.2.2). In our models, relative permeability decreases linearly as a function of decreasing liquid pore-water saturation to a minimum relative permeability value of 10^{-8} following Kurylyk et al. (2016), McKenzie et al. (2007), and McKenzie & Voss (2013). Alternative approaches to reducing hydraulic conductivity as a function of soil ice content are reviewed in Kurylyk & Watanabe (2013) and include theoretical approaches (e.g. Lebeau & Konrad, 2010; Watanabe & Flury, 2008) and

approaches based on the soil water characteristic curve for a drying soil (e.g. Brooks & Corey, 1964; Clapp & Hornberger, 1978; Painter et al., 2016; Van Genuchten, 1980). The onset of pore water freezing at a node occurs when temperature drops below 0 °C, and the proportion of frozen pore water increases linearly until a threshold temperature is reached (set here as -2 °C; McKenzie & Voss, 2013). At and below this threshold temperature, liquid water content is equal to a minimum allowed residual liquid water content (set here as 1% of pore space; McKenzie & Voss, 2013). Parameter values used in our simulation are defined in Table 1. For a full description of the model the reader is referred to McKenzie et al. (2007) and McKenzie & Voss (2013).

2.2.1 Domain and discretization

We created two separate domains intended to isolate the impact of groundwater flow on permafrost response to fire: a one-dimensional (1D) vertical column in which no groundwater flow occurs and a two-dimensional (2D) watershed cross-section with groundwater flow induced by a sloping land surface and a stream with an underlying talik at the downstream end of the domain (Figure 1). The 2D domain represents one half of a symmetrical catchment, and therefore it is not necessary to simulate the mirror hillslope on the other side of the stream (Evans et al., 2018; Ge et al., 2011). While we calibrate and validate our models using field data from the ARF to ensure our models are producing reasonable results, the archetypal domains are simplified representations of the Anaktuvuk River field sites intended to isolate groundwater impacts along the dominant hydrogeologic flow field (typically perpendicular to groundwater divides such as streams), thus allowing for a process-based exploration of fire impacts on groundwater-permafrost interactions (Voss, 2011a, 2011b; Zipper et al., 2018).

For both domains, our conceptual model was that of a two-layer (organic soil over mineral soil), fully saturated subsurface with homogeneous hydrologic and thermal properties within each layer. The organic soil layer ranged from 0.09 to 0.18 m in thickness depending on the scenario simulated (Table 2). We discretized the model into 120 vertical layers, increasing in thickness from 0.03 m at the land surface to 2.0 m at the bottom of the domain. The 2D domain was 41 nodes (40 elements) wide, with a uniform node spacing of 5 m. We tested this spacing to ensure changes in discretization did not have a strong impact on modeled thaw depth (Figure S2), though simulations with equal horizontal and vertical spacing were not conducted due to the high computational requirements for the size of our domain. The land surface of the 2D domain sloped from 25 m (at x=0 m) to 20 m (at x=200 m), to produce a 2.5% slope typical of the ARF region (Rocha & Shaver, 2011b). At the right edge of the 2D domain, we used a boundary condition representative of a stream with underlying talik (see Section 2.2.2).

In total, we constructed six unique model domains based on a factorial combination of model dimensionality (1D and 2D) and burn severity (UB, MB, and SB), which differed in the relative thickness of the organic and mineral soil layers (Table 2). In the following sections, we describe the boundary conditions (Section 2.2.2) which were applied to each domain to explore

parameter sensitivity (Section 2.2.3), and separate the impacts of changes in the water and energy balances (Section 2.3).

2.2.2 Inputs and boundary conditions

Model thermal and hydrologic boundary conditions for each domain were temporally constant on the bottom, left, and right sides (Figure 1). While specified heat flux bottom boundary conditions are often used for studies of permafrost-groundwater interactions (Evans & Ge, 2017; Kurylyk et al., 2016; McKenzie & Voss, 2013; Wellman et al., 2013), the focus of our study was exclusively shallow processes occurring in the active layer on a decadal timescale. Therefore, we decided to use a specified temperature bottom boundary condition at the zero annual temperature amplitude depth to reduce the size of the model domain and permit a more detailed sensitivity analysis (Section 2.2.3). We defined this temperature (-4.8 °C) and bottom boundary depth (20 m) based on ground temperature measurements at the Seabee Borehole (69.38°N, 152.18°W; 87 km from ARF sites), part of the Global Terrestrial Network for Permafrost database (Clow, 2014). Since the specified temperature is below the temperature at which minimum liquid saturation occurs, this bottom boundary will always be completely frozen and was simulated as a no-flow hydrologic boundary. Thermal and hydrologic boundary conditions on the right and left edges were no-flow based on the assumption of hydrologic symmetry around the stream at the center of the watershed (Section 2.2.1).

The upper thermal boundary condition was time-varying daily specified temperature based on soil temperature measurements from each of the three burn severity sites (Figure 2a). By using subsurface soil temperature as model input instead of temperature at the land surface, this boundary condition accounts for changes to the energy balance at the land surface, e.g. due to changes in albedo, snow insulation, and vegetation. From the time of flux tower installation at the ARF sites (June 2008) through the end of 2016, we used measured daily soil temperature at 0.05 m depth from each ARF site (Figure 2a) (Shaver and Rocha, 2015a-o). For the 2009-2016 period, there were 749, 480, and 343 days without data at the UB, MB, and SB sites, respectively, which primarily occurred during the winter. We gap-filled missing soil temperature data for the post-fire period using linear interpolation for gaps up to seven days in length. For gaps greater than seven days, which primarily occurred during January-June 2008 (prior to the installation of monitoring equipment), we used the average soil temperature for that day of year and burn severity from years where data were present.

The upper hydrologic boundary condition was a specified daily fluid source to the top layer of nodes, representing groundwater recharge (Figure 2b). This allowed the pressure at the land surface and the location of the water table to vary through time and between scenarios in response to changes in water fluxes, rather than prescribing a water table at the land surface which would create a constant hydraulic gradient. Groundwater recharge was estimated using a set fraction of daily combined rainfall and snowmelt from a temperature-based snowpack model (Walter et al., 2005) implemented within the *EcoHydRology* R package (Fuka et al., 2014) and

driven using daily meteorological data from the Toolik Field Station, which is ~40 km from the study sites (Environmental Data Center Team, 2017). Following Evans & Ge (2017), we used 20% of combined rainfall and snowmelt as a fluid source for the UB site. At the MB and SB sites, we decreased this value by 40% (resulting in a fluid source equal to 12% of combined daily rainfall and snowmelt) because flux tower measurements found that annual evapotranspiration at the MB and SB sites was consistently ~40-45% higher than the UB site; this has been attributed to increased surface water pooling associated with the thinner organic layer following fire (Rocha & Shaver, 2011b). Since this increase is consistent over the 2008-2016 period studied, we do not consider healing of the soil organic layer as an important factor in controlling differences in groundwater recharge. Healing occurs over longer timescales than the sub-decadal analysis performed here, and these effects are likely smaller than the large uncertainty in precipitation estimates in tundra settings (Liljedahl et al., 2017). Generalized pressure (or drain) boundary conditions were also implemented along the top boundary condition to prevent overpressuring (Evans & Ge, 2017). Therefore, not all of the fluid source provided will enter the groundwater flow system. For example, when the top nodes were frozen the drain nodes prevented excess water from entering the domain.

In the 2D domain, the rightmost 5 m (2 nodes) of the domain were specified pressure nodes at the land surface with a hydraulic head corresponding to 20.19 m and specified temperature of 4 °C, intended to represent a river or streambed with an underlying talik (Figure 1a). This head is equal to the land surface elevation 7.5 m from the edge of the domain, or halfway between the 2nd and 3rd nodes from the edge, in order to create a hydraulic gradient equal to the slope of the land surface at the stream (2.5%). We took outflow from these specified pressure nodes to represent groundwater discharge to the stream feature.

Initial pressure and temperature conditions for both 1D and 2D simulations were defined using a sequential spin-up approach. First, we used a steady-state simulation to estimate reasonable pressure and temperature fields to use as initial conditions for transient simulations. In the steady-state simulations, the upper hydrologic boundary condition was a specified pressure of 0 Pa (indicating a water table at the land surface) with a temperature of -8.43 °C (the mean annual soil temperature at the UB site). Following the steady-state simulations, we conducted a transient spin-up from 1998-2007 at a daily timestep with time-varying specified temperature and fluid source upper boundary conditions to allow the system to equilibrate to pre-fire conditions. During the 1998-2007 spin-up period prior to the installation of monitoring equipment at the ARF, we defined the upper thermal boundary conditions using daily soil temperature measurements at 0.087 m depth from the Toolik Soil Climate Research Station (Romanovsky et al., 2017). We then implemented the three different burn severity boundary conditions for the 2008-2016 period using data from the ARF sites (Figure 2). While post-fire data were available for the 2008-2016 period, we elected to exclude 2008 results from analysis because the flux towers were not installed until June 2008.

2.2.3 Sensitivity analysis and model evaluation

To examine the sensitivity of modeled active layer thickness to different thermal and hydrologic parameters under groundwater flow (2D) and no groundwater flow (1D) conditions, we conducted 5000 simulations while varying parameters using a Latin Hypercube Sample design (McKay et al., 1979) for each combination of dimensionality (1D and 2D) and the burn severity endmembers (UB and SB), for 20,000 simulations total. We varied six parameters (starred values in Table 1) representing hydrological and thermal properties of the subsurface: permeability, thermal conductivity, and porosity of the organic and mineral soil layers. Sampling used a uniform input distribution for each parameter, with permeability log-transformed prior to sampling.

Output from each simulation was daily temperature at each node, which we used to calculate daily thaw depth for comparison with field observations (Rocha & Shaver, 2015). Thaw depth is a particularly valuable measurement for model evaluation in permafrost settings, as it integrates soil temperature through and below the active layer. For the 2D simulations, we used thaw depth from the center of the domain (x=100 m) to minimize potential edge-effects of the no-flow boundary conditions at the left and right edges of the domain and the talik at the right edge. As noted in Section 2.2, our modeling approach uses a simplified domain to isolate key processes of interest (fire-induced changes to the water and energy balance). Therefore, the comparison with thaw depth measurements is intended to provide confidence that our model is representing active layer development at the Anaktuvuk River field site in a reasonable manner, but we are not intending to build a groundwater flow model specific to each site.

For a quantitative metric of model performance, we used the Kling-Gupta Efficiency (KGE; Gupta et al., 2009) as implemented in the *hydroGOF* package for R (Zambrano-Bigiarini, 2014). KGE modifies the widely-used Nash-Sutcliffe Efficiency (Nash & Sutcliffe, 1970) to provide an overall fit ($-\infty$ to 1.0) between observed and simulated timeseries, as well as separate measures of correlation (r), bias (β), and variability (α). A value of one corresponds to a perfect fit for both overall KGE and each decomposed metric. Given that our domain completely refreezes each winter, the maximum thaw depth for each year is equal to active layer thickness.

The relative importance of each parameter to total variability in active layer thickness and KGE was calculated separately for 1D and 2D cases using a generalized additive model (GAM) approach, as implemented in the *mgcv* package for R (Wood, 2003, 2011, 2017). GAMs are a type of generalized linear model integrating smoothing functions which are well-suited for nonlinear interactions between predictor and response variables. To estimate uncertainty, we used a bootstrapping approach in which we randomly sampled 75% of the simulation output 100 times to fit GAM models (Serbin et al., 2014; Zipper et al., 2016, 2017b; Zipper & Loheide, 2014). The proportion of variance explained by each parameter for each sample was calculated as the difference in deviance for a GAM excluding that parameter from the deviance in a GAM including all parameters, relative to the deviance from a null model.

Results from the sensitivity analysis were also used for model calibration and validation. We selected the parameters with the highest combined KGE between the UB and SB sites in which KGE at both sites was greater than 0.5. Calibrated model parameters were selected separately for the 1D and 2D domains. These calibrated parameters were then used to construct 1D and 2D models of the MB site for model validation.

2.3 Separating water and energy effects

To separate the effects of changes to the water and energy balance on permafrost thaw and active layer thickness, we conducted two additional simulations on the SB domain (Table 2). The first, which is intended to isolate the effects of fire-induced changes in the water balance on permafrost thaw, combined recharge from the SB site with soil temperature from the UB site (SB_W). The second was intended to isolate the effects of post-fire changes in the energy balance, and combined recharge from the UB site with soil temperature from the SB site (SB_E).

3 Results

3.1 Parameter sensitivity analysis

When groundwater is neglected (1D domain), active layer thickness is most responsive to changes in porosity of the mineral soil. There is a strong positive correlation between mean annual active layer thickness and porosity, which controls the bulk thermal conductivity of the subsurface (Figure 3a, top row). Comparing all parameters, variability in mineral soil porosity explains 72.9% (UB) and 90.9% (SB) of variability in active layer thickness (Figure 3b, top row). Soil thermal conductivity has a secondary effect on mean annual active layer thickness in the 1D simulations, with the relative importance of organic and mineral soil depending on burn severity (Figure 3, top row). At the UB site, the solid thermal conductivity of the organic soil layer explains 23.5% of variability in active layer thickness, while <1% of variability can be attributed to solid thermal conductivity of the mineral soil (Figure 3b, top row). In contrast, at the SB site, the relative importance of these two layers is reversed: mineral soil solid thermal conductivity contributes 5.6% of variability in active layer thickness, while organic soil solid thermal conductivity explains 3.0%. The greater influence of mineral soil properties at the SB site can be attributed to changes in the thickness of the organic soil layer following fire: the SB organic layer thickness is 50% that of the UB site (Table 2), thereby decreasing the influence of organic soil properties. The remaining properties evaluated (porosity of the organic layer, and permeability of both the mineral and organic layers) have a negligible effect on active layer thickness in the 1D domain (Figure 3, top row).

When lateral groundwater flow is simulated (2D domain), modeled sensitivity of the active layer to hydrologic properties increases, with greatest sensitivity to permeability of the organic soil in the UB domain, and porosity and permeability of the mineral soil for the SB domain (Figure 3, bottom row). Permeability of the organic soil layer explains 56.2% (UB) and 8.8% (SB) of variability in active layer thickness and the permeability of the mineral soil layer

contributes 6.8% (UB) and 27.2% (SB) of variability. Active layer thickness is also positively correlated with mineral soil porosity, which explains 9.7% (UB) and 44.4% (SB) of variability. The solid thermal conductivity of the mineral soil layer has a tertiary effect on active layer thickness, explaining 2.7% of variability, while the effects of all other properties are <1%. Comparing between burn severities, the relative importance of organic soil properties is higher at the UB site compared to the SB site as in the 1D domain due to the thicker organic layer at the UB site. There is also greater spread in active layer thickness results for the 2D domain compared to the 1D domain (Figure 3a), despite the same number of total model parameters, because thaw depth is sensitive to more parameters when groundwater flow is included (Figure 3b).

The impacts of groundwater on parameter sensitivity is also evident when evaluating model performance using KGE (Figure 4). In the 1D simulations, KGE is most sensitive to changes in organic thermal conductivity (59.6% of variability), mineral soil porosity (32.6%), and mineral soil thermal conductivity (21.3%); all other parameters explain <2% of total variability in KGE. In the 2D domain, mineral soil porosity and permeability are the dominant controls (25.2% and 23.7%, respectively), followed by organic permeability (10.8%); all other parameters explain <2% of variability in KGE. In reality, permeability is related to effective porosity (Carman, 1937; Kozeny, 1927); therefore, our results shed light on the relative importance of these two coupled factors.

3.2 Comparison to thaw observations

Using the results of the sensitivity analysis, we defined calibrated model parameters for the 1D and 2D domains. For each domain, we selected the set of parameters that produced the best KGE averaged between the UB and SB sites while exceeding 0.5 at both sites (red dots in Figure 4). For some parameters (e.g. thermal conductivity of the organic soil layer in the 2D domain), there was a large spread and no trend in the relationship between KGE and the parameter; this indicates that the modeled active layer thickness is not sensitive to this parameter, which is also reflected in GAM results (Figure 4b). We then simulated the MB site as a validation test (Figure 5). Since the response of KGE to both mineral soil porosity and permeability is linear with the calibrated parameters near one end, it may be argued that increasing the range of variability would better reproduce observations by identifying the point at which model performance peaks. However, given that the sampling encompasses a reasonable range of values for the silt loam soil type observed at the site (Carsel & Parrish, 1988; Romanovsky et al., 2017), we elected to not further expand the sensitivity analysis to avoid model overfitting.

Overall, both 1D and 2D calibrated models performed well for the calibration and validation sites (KGE>0.65; Figure 5). At the SB site, modeled thaw depth was underpredicted in later years, particularly 2016. This is associated with a notable decrease in annual soil temperature amplitude at the SB site, which behaves similarly to the UB site by the end of the

simulation period (Figure 2). However, the SB site still has the highest daily soil amplitude (not shown), indicating that subdaily thermal dynamics may be a key control on thaw depth not included in our modeling approach. Validation performance was weaker for the 1D domain than the 2D domain, primarily due to overpredicting thaw depth (β=1.093) and variability (α=1.284) in the 1D domain. Model performance assessed using KGE is better for the 2D calibrated model than the 1D calibrated model at all sites, potentially resulting from lateral groundwater flow in the 2D model (Section 3.1).

3.3 Response to water and energy balance changes

Following fire, interannual variability in the active layer thickness and thaw depth increased substantially. The four scenarios used to separate water and energy balance effects fall into two groups: scenarios with soil temperature inputs from the severe burn site (SB and SB_E) have deeper thaw (Figure 6a,c) and more variability (Figure 6b,d) than scenarios with soil temperature from the unburned site (UB and SB_W). These dynamics are comparable in both the absence (1D) and presence (2D) of groundwater flow and indicate that post-fire changes in active layer thickness are driven primarily by changes to the energy balance. However, these changes are relatively short-lived; by 2014 (seven years after the fire), seasonal patterns of permafrost thaw and active layer thickness are comparable across all simulations, as temperature at the UB and SB sites are comparable (Figure 2).

In contrast, both field measurements and model results indicate that spatial variability in thaw depth is highest at the unburned site and decreases as a function of burn severity (Figure 7). The coefficient of variation (C.V.) of thaw depth measurements is 13% greater at the UB site compared to the SB site (0.55 vs 0.48), with MB occupying an intermediate position (Figure 7b). Temporal patterns in thaw depth variance are consistent across sites, with the largest C.V. early in the summer when mean thaw depth is lowest, and a decreasing C.V. as time goes on (Figure 7c). Thus, while previous work documented an increase in thaw depth at these sites following fire (Rocha & Shaver, 2011b), relative variability in active layer thickness decreases due to fire in observed data, consistent with observed decreases in lateral thaw gradients shown in simulation results (Figure 7a).

Model results indicate that the decreased spatial variability in thaw depth following fire is driven by reduced groundwater flow (Figure 7a). In all scenarios including groundwater flow (2D domain), permafrost response varies along a gradient, with thinner active layers in the upland portion of the domain and thicker active layers in the lowland portion of the domain. Lateral thaw depth variability is largest in the scenarios without changes in the water balance due to fire: in the UB scenario active layer thickness is 0.24 m greater in the lowland region (x=180 m) compared to the upland region (x=20 m), a 57% increase, followed by the SB_E simulation (30% increase). Reductions in groundwater recharge due to fire decrease the degree of active layer thickness variability over the domain and reduce the difference between uplands and lowland regions to 26% in the SB_W scenario and 23% in the SB scenario.

3.4 Groundwater discharge to streams

Fire can impact groundwater discharge to surface water features (e.g. rivers and streams) by changing both the supply of water (via altered recharge) and the transmissivity of the subsurface (via altered active layer thickness). Here, fire led to an approximately 50% reduction in the quantity of water released from groundwater to the stream, with mean annual discharge decreasing from 3.78 m^3 in the UB scenario to 1.91 m^3 in the SB scenario (Figure 8), which is greater than the prescribed 40% decrease in groundwater recharge to the model (Figure 2). This decrease is due primarily to reduced groundwater recharge following fire: the lowest observed mean annual discharge (1.83 m^3) occurs in the SB_W scenario, when only groundwater recharge changes, while there is a slight reduction in mean annual discharge when only soil temperature changes (3.26 m^3 in the SB_E scenario). However, there was no observed shift in the timing of groundwater discharge to streams in either the onset of groundwater discharge in the spring or the day of peak discharge, despite the observed changes in the timing and magnitude of thaw between the different burn severities which controls groundwater recharge and flow in the subsurface (Figure 6).

4 Discussion

4.1 Importance of groundwater flow

Three lines of evidence support out hypothesis that heat transport via groundwater flow is a key control over permafrost response to fire. First, for a given set of parameters, active layer thickness is greater in simulations including groundwater flow (2D domain) compared to simulations neglecting groundwater flow (1D domain), indicating that lateral advection of sensible heat through groundwater flow enhances permafrost thaw relative to conduction-dominated simulations (Figures 3 and 4). Second, including groundwater flow increases the relative importance of hydraulic properties (soil permeability) and decreases the relative importance of thermal properties (soil thermal conductivity), indicating that subsurface heat transport by advection is of greater importance than heat transport by conduction (Figures 3 and 4). Third, model calibration and validation performance is better in the 2D simulations where groundwater flow is included compared to the 1D simulations where groundwater flow is ignored (Figure 5), indicating that including groundwater flow is a more accurate representation of real-world conditions. Combined, these results indicate that lateral heat transport through the active layer via groundwater flow is an important but underappreciated component of post-fire permafrost dynamics, and the relative importance of advective heat transport will likely be greater where groundwater flow rates are higher (e.g. more conductive sediments or a higher hydraulic gradient).

While previous work has shown that heat transport via lateral groundwater flow can be a positive feedback to permafrost degradation (e.g. Bense et al., 2009, 2012; Connon et al., 2018, 2014; Kurylyk et al., 2016), this is the first study to demonstrate that advective heat transport is a

key driver of the permafrost response to fire. Importantly, it suggests that spatial variability in the ecohydrological response to fire, a key research priority for disturbance hydrology (Mirus et al., 2017), may be in part driven by groundwater flow which enhances permafrost degradation in lowland areas (Figure 7). Based on our results, we suggest that the degree to which fire effects can be transported laterally via groundwater flow are strongly dependent on post-fire hydraulic gradients and soil properties. Given that both the vertical water balance and soil hydraulic properties may be modified by fire (Kettridge et al., 2012, 2017; Lukenbach et al., 2016; Semenova et al., 2015; Sherwood et al., 2013; Thompson et al., 2014; Thompson & Waddington, 2013), this represents a potential post-fire feedback which merits further investigation. For example, since deeper organic soils are often less conductive than near-surface organic soils, burning off the near-surface soil would lead to a decrease in the average hydraulic conductivity of the organic soil layer (Hinzman et al., 1991; Neilson et al., 2018; Quinton et al., 2008).

4.2 Active layer thickness response to water and energy balance changes

We also demonstrate that changes to the water and energy balance have opposite effects on permafrost thaw depth. Changes to the energy balance increase both conductive and advective energy transport into the subsurface by increasing near-surface soil temperatures which act as an upper boundary to the system (Figure 2), leading to an increase in active layer thickness in both SB and SB_E scenarios relative to the UB scenario (Figure 6). In contrast, changes to the water balance lead to a reduction in groundwater recharge, which reduces advective heat transport and decreases active layer thickness in the SB_W scenario relative to the UB scenario (Figure 6).

These results indicate that changes to the energy balance are the dominant control over the thickness of the active layer following fire as evidenced by the similarity in thaw depth between simulations for the SB site and the SB_E simulation which isolated changes to the energy balance (Figure 6, 7). While the dominance of energy balance changes may seem to contradict the strong sensitivity of modeled thaw dynamics to hydrological parameters (Figures 3 and 4), these results are reconciled by noting that heat transport via advection is a function of both the energy content of groundwater (a function of soil temperature) and the magnitude of groundwater flow (a function of recharge and active layer thickness). Therefore, changes in the energy balance can be the dominant driver of permafrost thaw dynamics as observed in previous studies (Brown et al., 2016), even where groundwater flow is an important process. As warming in high-latitude regions shifts the timing and magnitude of spring snowmelt, changes in to the water balance may increase in importance (Bring et al., 2016; Lique et al., 2016), in particular at sites with finer-grained mineral soils which are able to hold more unfrozen water even at subzero temperatures, buffering permafrost from changes in air temperature (Nicolsky & Romanovsky, 2018).

In contrast, changes to the water balance are the dominant control over spatial variability in active layer thickness as evidenced by greater lateral heterogeneity in active layer thickness for the SB site and the SB_W simulation which isolated changes to groundwater recharge rates

(Figure 7). This variability is not random, but a function of landscape position with greater differences in active layer thickness between uplands (less thaw) and lowlands (more thaw) in simulations in which there is more groundwater flow. This is consistent with field observations showing a decrease in the relative variability of thaw depth following fire (Figure 7b-c). While our study focused on a continuous permafrost environment, thaw in lowland areas may be particularly important in areas of discontinuous permafrost where it is likely to increase subsurface hydrologic connectivity which can induce ecologically significant land cover transitions (Connon et al., 2014; Kurylyk et al., 2016; Quinton et al., 2011).

4.3 Baseflow response to water and energy balance changes

We show that the supply of water (groundwater recharge) is the key control over post-fire changes in baseflow (Figure 8), leading to up to ~50% decreases in annual groundwater discharge in the SB and SB_W scenarios. Changes in transmissivity appear to have little effect, as the SB_E scenario which had the largest increase in active layer thickness (Figures 6, 7) has a negligible change in groundwater discharge to the stream under the conditions simulated (Figure 8). Changes in recharge alone are not sufficient to explain the simulated 50% decrease in groundwater discharge, as fire led to only a 40% reduction in groundwater recharge (Figure 2). Therefore, we suggest that a weakening of the hydraulic gradient following fire, caused by a reduction in groundwater recharge and advective heat transport leading to smaller differences in active layer thickness between upslope and downslope portions of the domain (Figure 7a), may also be an important driver of changes in baseflow following fire.

Relatively little work has examined changes in groundwater-surface water interactions following fire in permafrost environments. In Alaska, post-fire flow during rain events was enhanced by the increased thickness of the active layer (Petrone et al., 2007). While our study does not examine response to individual precipitation events, the observed increases in active layer thickness resulting from fire (e.g. Figure 7a) provides a mechanism for these increases in stormflow by providing more space in the near-surface soil layers through which water can flow. In contrast, in our simulations lower water inputs led to a net decrease in groundwater discharge to streams. At larger scales, previous work has shown that forest fires cause a slight increase in streamflow in Arctic settings, though this signal is small relative to changes in atmospheric moisture transport (McClelland et al., 2004).

We suggest that the impacts of fire on groundwater discharge to streams depend strongly on local site characteristics, given the substantial uncertainty regarding post-fire changes to the water and energy balances. For instance, previous work has demonstrated that in settings where permafrost thaw leads to enhanced subsurface connectivity (e.g. the talik grows deep enough to connect to a subpermafrost aquifer or form a lateral, perennially unfrozen talik), groundwater flow processes can exert a major control (Bense et al., 2012; Lamontagne-Hallé et al., 2018). Thus, the impacts of fire on baseflow may be stronger in regions of discontinuous permafrost with more dynamic changes in hydrologic connectivity (Connon et al., 2014, 2015; Walvoord et

al., 2012). Furthermore, at our study site fire was associated with an increase in evapotranspiration and concomitant reduction in groundwater recharge (Rocha & Shaver, 2011b); work elsewhere has documented both increases (Thompson et al., 2014) and decreases (Liu et al., 2005) in evapotranspiration following fire in cold regions, indicating that advances to our understanding of the land surface water and energy balance are necessary to improve boundary representation in subsurface models.

4.4 Study limitations

Despite the strong model performance when compared to field observations (Figure 5), there are several limitations to our approach which may affect our results. First, freeze/thaw processes in our model only consider freezing of water within existing pore space, and therefore thermo-hydro-mechanical processes such as thermokarst development and ice lensing are not simulated. In particular, our two-dimensional model does not include three-dimensional water and energy transport processes that can occur in permafrost settings such as 'water tracks', which are subsurface drainage channels through which water can flow rapidly (Chapin et al., 1988; McNamara et al., 1998). Since water tracks are associated with rapid water transport, warmer soil, and deeper active layer thickness than surrounding areas (Curasi et al., 2016; Hastings et al., 1989), they would likely enhance the importance of heat transport via advection which we document here. Similarly, our model is only of the subsurface, and therefore does not simulate ponding at the land surface which may occur during snowmelt or precipitation events if there is insufficient infiltration capacity; this limitation likely underestimates both the quantity and duration of groundwater recharge, particularly during spring snowmelt, and may dampen effects of changes in the water balance.

Additionally, our archetypal modeling approach simulates saturated flow with homogeneous subsurface properties. Variably saturated processes may be important, particularly in high-porosity soils in which air-filled pore space can act as a thermal buffer (Kettridge et al., 2012; Quinton et al., 2000). Since our upper thermal boundary condition is based on soil temperature measurements at a depth of 5 cm, it accounts for near-surface drying but may be inaccurate if the water table falls below the soil temperature sensor which would likely occur in late summer. Previous work in the ARF region found that the mineral soil layer tends to stay saturated, while the organic layer dries seasonally (Hinzman et al., 1991). Therefore, if we considered variably saturated conditions, the sensitivity of active layer thickness to the porosity of the organic layer may increase, as porosity is the main control over the potential amount of air-filled pore space. If organic soils were to dry, the relative importance of vertical heat transport would decrease due to reduced conduction through air-filled pore space, while groundwater flow would still be driving advective heat transport in the unfrozen saturated zone (Lamontagne-Hallé et al., 2018) through which there is substantial groundwater flow and groundwater-surface water exchange even during partially unsaturated conditions (Neilson et al., 2018). Therefore, it is likely that lateral groundwater flow would be an even more important part of the permafrost response to fire if our models considered variably saturated conditions.

We also used a homogeneous temperature-liquid water content relationship as defined by the minimum liquid saturation and temperature below which minimum liquid saturation occurs (Table 1). However, these values are likely to vary as a function of soil texture, with higher liquid saturation at low temperatures in finer-grained materials (Kurylyk & Watanabe, 2013; Nicolsky & Romanovsky, 2018; Tarnawski & Wagner, 1993; Van Genuchten, 1980). Since liquid water has a lower thermal conductivity than ice, using a higher value of minimum liquid saturation would decrease the bulk thermal conductivity in the subsurface during the winter months and during spring snowmelt, potentially further diminishing the relative importance of heat transport via conduction. Finally, our specified boundary condition intended to represent a streambed is simplified and does not include temporal dynamics (e.g. high water levels during spring freshet, seasonal changes in temperature) which may influence stream-aquifer interactions. Additional field measurements such as stream stage, stream temperature, and water table gradient in the hillslope areas may help resolve some of these uncertainties and aid in the construction of a site-specific model.

While our modeling approach may neglect some locally-important processes, the objective of our study was to isolate the effects of groundwater flow on post-fire permafrost distribution. Our archetypal approach to groundwater modeling provides information about the fundamental processes controlling system dynamics, and therefore provides more generalizable information than highly parameterized models. By making these assumptions, we were able to isolate the role of groundwater, providing a more generalized understanding of flow processes in variably frozen porous media, which physical properties and model parameters most strongly influence the response of subsurface processes to fire, and how fire-induced changes are able to propagate laterally through groundwater flow.

5 Conclusions

In this study, we quantified the importance of groundwater flow to permafrost thaw following fire. Our results demonstrate that hydrogeological processes are a key control over permafrost dynamics following fire, and that neglecting lateral water and heat transport may lead to overestimation of the importance of thermal properties. We also show that an increase in energy input to the subsurface following fire is the primary driver of increases in active layer thickness, and permafrost thaw is enhanced by advective heat transport via groundwater flow. However, changes to the water balance are the key control over post-fire spatial heterogeneity in thaw depth and groundwater discharge to surface water features such as streams. These results show that groundwater flow and associated water and energy transport processes are essential to understanding the impacts of fire on permafrost dynamics, as well as changes in biogeochemical cycles which are affected by hydrological processes.

Acknowledgments and Data

SCZ, PLH, and JMM were funded by the Natural Sciences and Engineering Research Council of Canada (NSERC) and the McGill University Trottier Institute for Science and Public Policy. AVR and data collection were funded by NSF grant #1556772 to the University of Notre Dame. This manuscript has been improved by discussions with Tom Gleeson, Yueyang Jiang, and Barret Kurylyk, as well as constructive feedback from John Buffington, Sebastian Westermann, and two anonymous reviewers. Anaktuvuk River data sets were provided by the Arctic LTER (Rocha and Shaver, 2015; Shaver and Rocha, 2015a-o). Model files, output, and analysis scripts are available at https://doi.org/10.6084/m9.figshare.7070177. This material is based upon work supported by the National Science Foundation under grants #DEB-981022, 9211775, 8702328; #OPP-9911278, 9911681, 9732281, 9615411, 9615563, 9615942, 9615949, 9400722, 9415411, 9318529; #BSR 9019055, 8806635, 8507493. Meteorological datasets were provided by the Toolik Field Station Environmental Data Center (Environmental Data Center Team, 2017) based upon work supported by the National Science Foundation under grants #455541 and 1048361. All analyses were performed using R 3.4.0 (R Core Team, 2017) and graphics made using ggplot2 (Wickham, 2009) and InkScape (The Inkscape Team, 2015).

References

Abbott, B. W., Jones, J. B., Schuur, E. A. G., III, F. S. C., Bowden, W. B., Bret-Harte, M. S., … Zimov, S. (2016). Biomass offsets little or none of permafrost carbon release from soils, streams, and wildfire: an expert assessment. *Environmental Research Letters*, *11*(3), 034014. https://doi.org/10.1088/1748-9326/11/3/034014

Balshi, M. S., McGuire, A. D., Zhuang, Q., Melillo, J., Kicklighter, D. W., Kasischke, E., … Shvidenko, A. (2007). The role of historical fire disturbance in the carbon dynamics of the pan-boreal region: A process-based analysis. *Journal of Geophysical Research-Biogeosciences*, *112*(G2), G02029. https://doi.org/10.1029/2006JG000380

Bense, V. F., Ferguson, G., & Kooi, H. (2009). Evolution of shallow groundwater flow systems in areas of degrading permafrost. *Geophysical Research Letters*, *36*(22), L22401. https://doi.org/10.1029/2009GL039225

Bense, V. F., Kooi, H., Ferguson, G., & Read, T. (2012). Permafrost degradation as a control on hydrogeological regime shifts in a warming climate. *Journal of Geophysical Research-Earth Surface*, *117*, F03036. https://doi.org/10.1029/2011JF002143

Bret-Harte, M. S., Mack, M. C., Shaver, G. R., Huebner, D. C., Johnston, M., Mojica, C. A., … Reiskind, J. A. (2013). The response of Arctic vegetation and soils following an unusually severe tundra fire. *Philosophical Transactions of the Royal Society B-Biological Sciences*, *368*(1624), UNSP 20120490. https://doi.org/10.1098/rstb.2012.0490

Bring, A., Fedorova, I., Dibike, Y., Hinzman, L., Mard, J., Mernild, S. H., … Woo, M.-K. (2016). Arctic terrestrial hydrology: A synthesis of processes, regional effects, and research challenges. *Journal of Geophysical Research-Biogeosciences*, *121*(3), 621–649. https://doi.org/10.1002/2015JG003131

Brooks, R. H., & Corey, A. T. (1964). *Hydraulic properties of porous media* (Hydrology Papers No. 3). Fort Collins: Colorado State University.

Brown, D. R. N., Jorgenson, M. T., Kielland, K., Verbyla, D. L., Prakash, A., & Koch, J. C. (2016). Landscape Effects of Wildfire on Permafrost Distribution in Interior Alaska Derived from Remote Sensing. *Remote Sensing*, *8*(8), 654. https://doi.org/10.3390/rs8080654

Brown, D. R. N., Jorgenson, M. T., Douglas, T. A., Romanovsky, V. E., Kielland, K., Hiemstra, C., … Ruess, R. W. (2015). Interactive effects of wildfire and climate on permafrost degradation in Alaskan lowland forests. *Journal of Geophysical Research-Biogeosciences*, *120*(8), 1619–1637. https://doi.org/10.1002/2015JG003033

Campbell, G. S., & Norman, J. M. (2000). *An Introduction to Environmental Biophysics* (2nd ed.). Springer.

Carman, P. C. (1937). Fluid flow through granular beds. *Trans. Inst. Chem. Eng.*, *15*, 150–166.

Carsel, R. F., & Parrish, R. S. (1988). Developing joint probability-distributions of soil-water retention characteristics. *Water Resources Research*, *24*(5), 755–769. https://doi.org/10.1029/WR024i005p00755

Chapin, F. S., Fetcher, N., Kielland, K., Everett, K. R., & Linkins, A. E. (1988). Productivity and Nutrient Cycling of Alaskan Tundra: Enhancement by Flowing Soil Water. *Ecology*, *69*(3), 693–702. https://doi.org/10.2307/1941017

Chipman, M. L., & Hu, F. S. (2017). Linkages Among Climate, Fire, and Thermoerosion in Alaskan Tundra Over the Past Three Millennia. *Journal of Geophysical Research: Biogeosciences*, *122*(12), 3362–3377. https://doi.org/10.1002/2017JG004027

Clapp, R. B., & Hornberger, G. M. (1978). Empirical equations for some soil hydraulic properties. *Water Resources Research*, *14*(4), 601–604. https://doi.org/10.1029/WR014i004p00601

Clow, G. D. (2014). Global Terrestrial Network for Permafrost - Seabee. Retrieved February 27, 2017, from http://gtnpdatabase.org/boreholes/view/812

Connon, R. F., Quinton, W. L., Craig, J. R., & Hayashi, M. (2014). Changing hydrologic connectivity due to permafrost thaw in the lower Liard River valley, NWT, Canada. *Hydrological Processes*, *28*(14), 4163–4178. https://doi.org/10.1002/hyp.10206

Connon, R. F., Quinton, W. L., Craig, J. R., Hanisch, J., & Sonnentag, O. (2015). The hydrology of interconnected bog complexes in discontinuous permafrost terrains. *Hydrological Processes*, *29*(18), 3831–3847. https://doi.org/10.1002/hyp.10604

Connon, R., Devoie, É., Hayashi, M., Veness, T., & Quinton, W. (2018). The Influence of Shallow Taliks on Permafrost Thaw and Active Layer Dynamics in Subarctic Canada. *Journal of Geophysical Research: Earth Surface*, *123*(2), 281–297. https://doi.org/10.1002/2017JF004469

Curasi, S. R., Loranty, M. M., & Natali, S. M. (2016). Water track distribution and effects on carbon dioxide flux in an eastern Siberian upland tundra landscape. *Environmental Research Letters*, *11*(4), 045002. https://doi.org/10.1088/1748-9326/11/4/045002

De Baets, S., van de Weg, M. J., Lewis, R., Steinberg, N., Meersmans, J., Quine, T. A., … Hartley, I. P. (2016). Investigating the controls on soil organic matter decomposition in tussock tundra soil and permafrost after fire. *Soil Biology and Biochemistry*, *99*, 108–116. https://doi.org/10.1016/j.soilbio.2016.04.020

Environmental Data Center Team. (2017). Meteorological Monitoring program at Toolik, Alaska. Toolik Field Station, Institute of Arctic Biology, University of Alaska Farbanks, Fairbanks, AK 99775. Retrieved March 27, 2017, from http://toolik.alaska.edu/edc/abiotic_monitoring/data_query.php

Evans, S. G., & Ge, S. (2017). Contrasting hydrogeologic responses to warming in permafrost and seasonally frozen ground hillslopes. *Geophysical Research Letters*, *44*(4), 2016GL072009. https://doi.org/10.1002/2016GL072009

Evans, S. G., Ge, S., Voss, C. I., & Molotch, N. P. (2018). The Role of Frozen Soil in Groundwater Discharge Predictions for Warming Alpine Watersheds. *Water Resources Research*, *54*(3), 1599–1615. https://doi.org/10.1002/2017WR022098

Flannigan, M. D., Logan, K. A., Amiro, B. D., Skinner, W. R., & Stocks, B. J. (2005). Future area burned in Canada. *Climatic Change*, *72*(1–2), 1–16. https://doi.org/10.1007/s10584-005-5935-y

Fuka, D., Walter, M., Archibald, J., Steenhuis, J., & Easton, Z. (2014). EcoHydRology: A community modeling foundation for Eco-Hydrology (Version 0.4.12). Retrieved from https://CRAN.R-project.org/package=EcoHydRology

Ge, S., McKenzie, J., Voss, C., & Wu, Q. (2011). Exchange of groundwater and surface-water mediated by permafrost response to seasonal and long term air temperature variation. *Geophysical Research Letters*, *38*(14), L14402. https://doi.org/10.1029/2011GL047911

Grenier, C., Anbergen, H., Bense, V., Chanzy, Q., Coon, E., Collier, N., … Voss, C. (2018). Groundwater flow and heat transport for systems undergoing freeze-thaw: Intercomparison of numerical simulators for 2D test cases. *Advances in Water Resources*, *114*, 196–218. https://doi.org/10.1016/j.advwatres.2018.02.001

Gupta, H. V., Kling, H., Yilmaz, K. K., & Martinez, G. F. (2009). Decomposition of the mean squared error and NSE performance criteria: Implications for improving hydrological modelling. *Journal of Hydrology*, *377*(1), 80–91. https://doi.org/10.1016/j.jhydrol.2009.08.003

Hastings, S. J., Luchessa, S. A., Oechel, W. C., & Tenhunen, J. D. (1989). Standing biomass and production in water drainages of the foothills of the Philip Smith Mountains, Alaska. *Ecography*, *12*(3), 304–311. https://doi.org/10.1111/j.1600-0587.1989.tb00850.x

Higuera, P. E., Brubaker, L. B., Anderson, P. M., Brown, T. A., Kennedy, A. T., & Hu, F. S. (2008). Frequent fires in ancient shrub tundra: Implications of paleorecords for Arctic environmental change. *PLoS ONE*, *3*(3), e0001744. https://doi.org/10.1371/journal.pone.0001744

Hinzman, L. D., Kane, D. L., Gieck, R. E., & Everett, K. R. (1991). Hydrologic and thermal properties of the active layer in the Alaskan Arctic. *Cold Regions Science and Technology*, *19*(2), 95–110. https://doi.org/10.1016/0165-232X(91)90001-W

Hu, F. S., Higuera, P. E., Walsh, J. E., Chapman, W. L., Duffy, P. A., Brubaker, L. B., & Chipman, M. L. (2010). Tundra burning in Alaska: Linkages to climatic change and sea ice retreat. *Journal of Geophysical Research: Biogeosciences*, *115*(G4), G04002. https://doi.org/10.1029/2009JG001270

Hu, F. S., Higuera, P. E., Duffy, P., Chipman, M. L., Rocha, A. V., Young, A. M., … Dietze, M. C. (2015). Arctic tundra fires: natural variability and responses to climate change. *Frontiers in Ecology and the Environment*, *13*(7), 369–377. https://doi.org/10.1890/150063

Iwahana, G., Harada, K., Uchida, M., Tsuyuzaki, S., Saito, K., Narita, K., … Hinzman, L. D. (2016). Geomorphological and geochemistry changes in permafrost after the 2002 tundra wildfire in Kougarok, Seward Peninsula, Alaska. *Journal of Geophysical Research: Earth Surface*, *121*(9), 2016JF003921. https://doi.org/10.1002/2016JF003921

Jafarov, E. E., Romanovsky, V. E., Genet, H., McGuire, A. D., & Marchenko, S. S. (2013). The effects of fire on the thermal stability of permafrost in lowland and upland black spruce forests of interior Alaska in a changing climate. *Environmental Research Letters*, *8*(3), 035030. https://doi.org/10.1088/1748-9326/8/3/035030

Jiang, Y., Rastetter, E. B., Shaver, G. R., Rocha, A. V., Zhuang, Q., & Kwiatkowski, B. L. (2017). Modeling long-term changes in tundra carbon balance following wildfire, climate change, and potential nutrient addition. *Ecological Applications*, *27*(1), 105–117. https://doi.org/10.1002/eap.1413

Jiang, Y., Zhuang, Q., & O'Donnell, J. A. (2012). Modeling thermal dynamics of active layer soils and near-surface permafrost using a fully coupled water and heat transport model. *Journal of Geophysical Research: Atmospheres*, *117*(D11), D11110. https://doi.org/10.1029/2012JD017512

Jiang, Y., Rastetter, E. B., Rocha, A. V., Pearce, A. R., Kwiatkowski, B. L., & Shaver, G. . . (2015a). Modeling carbon–nutrient interactions during the early recovery of tundra after fire. *Ecological Applications*, *25*(6), 1640–1652. https://doi.org/10.1890/14-1921.1

Jiang, Y., Rocha, A. V., O'Donnell, J. A., Drysdale, J. A., Rastetter, E. B., Shaver, G. R., & Zhuang, Q. (2015b). Contrasting soil thermal responses to fire in Alaskan tundra and boreal forest. *Journal of Geophysical Research-Earth Surface*, *120*(2), 363–378. https://doi.org/10.1002/2014JF003180

Jones, B. M., Kolden, C. A., Jandt, R., Abatzoglou, J. T., Urban, F., & Arp, C. D. (2009). Fire Behavior, Weather, and Burn Severity of the 2007 Anaktuvuk River Tundra Fire, North Slope, Alaska. *Arctic, Antarctic, and Alpine Research*, *41*(3), 309–316. https://doi.org/10.1657/1938-4246-41.3.309

Jones, B. M., Grosse, G., Arp, C. D., Miller, E., Liu, L., Hayes, D. J., & Larsen, C. F. (2015). Recent Arctic tundra fire initiates widespread thermokarst development. *Scientific Reports*, *5*, 15865. https://doi.org/10.1038/srep15865

Kasischke, E. S., & Johnstone, J. F. (2005). Variation in postfire organic layer thickness in a black spruce forest complex in interior Alaska and its effects on soil temperature and moisture. *Canadian Journal of Forest Research-Revue Canadienne De Recherche Forestiere*, *35*(9), 2164–2177. https://doi.org/10.1139/X05-159

Kasischke, E. S., Bourgeau-Chavez, L. L., & Johnstone, J. F. (2007). Assessing spatial and temporal variations in surface soil moisture in fire-disturbed black spruce forests in Interior Alaska using spaceborne synthetic aperture radar imagery - Implications for post-fire tree recruitment. *Remote Sensing of Environment*, *108*(1), 42–58. https://doi.org/10.1016/j.rse.2006.10.020

Kettridge, N., Thompson, D. K., & Waddington, J. M. (2012). Impact of wildfire on the thermal behavior of northern peatlands: Observations and model simulations. *Journal of Geophysical Research: Biogeosciences*, *117*(G2), G02014. https://doi.org/10.1029/2011JG001910

Kettridge, N., Lukenbach, M. C., Hokanson, K. J., Hopkinson, C., Devito, K. J., Petrone, R. M., … Waddington, J. M. (2017). Low Evapotranspiration Enhances the Resilience of Peatland Carbon Stocks to Fire. *Geophysical Research Letters*, *44*(18), 2017GL074186. https://doi.org/10.1002/2017GL074186

Kozeny, J. (1927). Uber kapillare leitung der wasser in boden. *Royal Academy of Science, Vienna, Proc. Class I*, *136*, 271–306.

Kurylyk, B. L., Hayashi, M., Quinton, W. L., McKenzie, J. M., & Voss, C. I. (2016). Influence of vertical and lateral heat transfer on permafrost thaw, peatland landscape transition, and groundwater flow. *Water Resources Research*, *52*(2), 1286–1305. https://doi.org/10.1002/2015WR018057

Kurylyk, B. L., & Watanabe, K. (2013). The mathematical representation of freezing and thawing processes in variably-saturated, non-deformable soils. *Advances in Water Resources*, *60*, 160–177. https://doi.org/10.1016/j.advwatres.2013.07.016

Lamontagne-Hallé, P., McKenzie, J. M., Kurylyk, B. L., & Zipper, S. C. (2018). Changing groundwater discharge dynamics in permafrost regions. *Environmental Research Letters*, *13*(8), 084017. https://doi.org/10.1088/1748-9326/aad404

Lebeau, M., & Konrad, J.-M. (2010). A new capillary and thin film flow model for predicting the hydraulic conductivity of unsaturated porous media. *Water Resources Research*, *46*(12). https://doi.org/10.1029/2010WR009092

Liljedahl, A. K., Hinzman, L. D., Kane, D. L., Oechel, W. C., Tweedie, C. E., & Zona, D. (2017). Tundra water budget and implications of precipitation underestimation. *Water Resources Research*, *53*(8), 6472–6486. https://doi.org/10.1002/2016WR020001

Lique, C., Holland, M. M., Dibike, Y. B., Lawrence, D. M., & Screen, J. A. (2016). Modeling the Arctic freshwater system and its integration in the global system: Lessons learned and future challenges. *Journal of Geophysical Research-Biogeosciences*, *121*(3), 540–566. https://doi.org/10.1002/2015JG003120

Liu, H. P., Randerson, J. T., Lindfors, J., & Chapin, F. S. (2005). Changes in the surface energy budget after fire in boreal ecosystems of interior Alaska: An annual perspective. *Journal of Geophysical Research-Atmospheres*, *110*(D13), D13101. https://doi.org/10.1029/2004JD005158

Lukenbach, M. C., Devito, K. J., Kettridge, N., Petrone, R. M., & Waddington, J. M. (2016). Burn severity alters peatland moss water availability: implications for post-fire recovery. *Ecohydrology*, *9*(2), 341–353. https://doi.org/10.1002/eco.1639

Mack, M. C., Bret-Harte, M. S., Hollingsworth, T. N., Jandt, R. R., Schuur, E. A. G., Shaver, G. R., & Verbyla, D. L. (2011). Carbon loss from an unprecedented Arctic tundra wildfire. *Nature*, *475*(7357), 489–492. https://doi.org/10.1038/nature10283

McClelland, J. W., Holmes, R. M., Peterson, B. J., & Stieglitz, M. (2004). Increasing river discharge in the Eurasian Arctic: Consideration of dams, permafrost thaw, and fires as potential agents of change. *Journal of Geophysical Research-Atmospheres*, *109*(D18), D18102. https://doi.org/10.1029/2004JD004583

McKay, M. D., Beckman, R. J., & Conover, W. J. (1979). A Comparison of Three Methods for Selecting Values of Input Variables in the Analysis of Output from a Computer Code. *Technometrics*, *21*(2), 239–245. https://doi.org/10.2307/1268522

McKenzie, J. M., Voss, C. I., & Siegel, D. I. (2007). Groundwater flow with energy transport and water–ice phase change: Numerical simulations, benchmarks, and application to freezing in peat bogs. *Advances in Water Resources*, *30*(4), 966–983. https://doi.org/10.1016/j.advwatres.2006.08.008

McKenzie, J. M., & Voss, C. I. (2013). Permafrost thaw in a nested groundwater-flow system. *Hydrogeology Journal*, *21*(1), 299–316. https://doi.org/10.1007/s10040-012-0942-3

McNamara, J. P., Kane, D. L., & Hinzman, L. D. (1998). An analysis of streamflow hydrology in the Kuparuk River Basin, Arctic Alaska: a nested watershed approach. *Journal of Hydrology*, *206*(1), 39–57. https://doi.org/10.1016/S0022-1694(98)00083-3

Minsley, B. J., Pastick, N. J., Wylie, B. K., Brown, D. R. N., & Kass, M. A. (2016). Evidence for nonuniform permafrost degradation after fire in boreal landscapes. *Journal of Geophysical Research-Earth Surface*, *121*(2), 320–335. https://doi.org/10.1002/2015JF003781

Mirus, B. B., Ebel, B. A., Mohr, C. H., & Zegre, N. (2017). Disturbance Hydrology: Preparing for an Increasingly Disturbed Future. *Water Resources Research*, *53*(12), 10007–10016. https://doi.org/10.1002/2017WR021084

Naasz, R., Michel, J.-C., & Charpentier, S. (2005). Measuring Hysteretic Hydraulic Properties of Peat and Pine Bark using a Transient Method. *Soil Science Society of America Journal*, *69*(1), 13–22. https://doi.org/10.2136/sssaj2005.0013

Nash, J. E., & Sutcliffe, J. V. (1970). River flow forecasting through conceptual models part I — A discussion of principles. *Journal of Hydrology*, *10*(3), 282–290. https://doi.org/10.1016/0022-1694(70)90255-6

Neilson, B. T., Cardenas, M. B., O'Connor, M. T., Rasmussen, M. T., King, T. V., & Kling, G. W. (2018). Groundwater flow and exchange across the land surface explain carbon export patterns in continuous permafrost watersheds. *Geophysical Research Letters*, *45*(15), 7596–7605. https://doi.org/10.1029/2018GL078140

Nicolsky, D. J., & Romanovsky, V. E. (2018). Modeling Long-Term Permafrost Degradation. *Journal of Geophysical Research: Earth Surface*. https://doi.org/10.1029/2018JF004655

Painter, S. L., Coon, E. T., Atchley, A. L., Berndt, M., Garimella, R., Moulton, J. D., … Wilson, C. J. (2016). Integrated surface/subsurface permafrost thermal hydrology: Model formulation and proof-of-concept simulations. *Water Resources Research*, *52*(8), 6062–6077. https://doi.org/10.1002/2015WR018427

Petrone, K. C., Hinzman, L. D., Shibata, H., Jones, J. B., & Boone, R. D. (2007). The influence of fire and permafrost on sub-arctic stream chemistry during storms. *Hydrological Processes*, *21*(4), 423–434. https://doi.org/10.1002/hyp.6247

Quinton, W. L., Hayashi, M., & Carey, S. K. (2008). Peat hydraulic conductivity in cold regions and its relation to pore size and geometry. *Hydrological Processes*, *22*(15), 2829–2837. https://doi.org/10.1002/hyp.7027

Quinton, W. L., Hayashi, M., & Chasmer, L. E. (2011). Permafrost-thaw-induced land-cover change in the Canadian subarctic: implications for water resources. *Hydrological Processes*, *25*(1), 152–158. https://doi.org/10.1002/hyp.7894

Quinton, W. L., Gray, D. M., & Marsh, P. (2000). Subsurface drainage from hummock-covered hillslopes in the Arctic tundra. *Journal of Hydrology*, *237*(1), 113–125. https://doi.org/10.1016/S0022-1694(00)00304-8

R Core Team. (2018). R: A language and environment for statistical computing (Version 3.4.4). Vienna, Austria: R Foundation for Statistical Computing. Retrieved from https://www.R-project.org/

Rocha, A. V., Shaver, G. R., & Hobbie, J. (2008a). AmeriFlux US-An1 Anaktuvuk River Moderate Burn. Retrieved February 27, 2017, from http://dx.doi.org/10.17190/AMF/1246143

Rocha, A. V., Shaver, G. R., & Hobbie, J. (2008b). AmeriFlux US-An1 Anaktuvuk River Severe Burn. Retrieved February 27, 2017, from http://dx.doi.org/10.17190/AMF/1246142

Rocha, A. V., Shaver, G. R., & Hobbie, J. (2008c). AmeriFlux US-An1 Anaktuvuk River Unburned. Retrieved February 27, 2017, from http://dx.doi.org/10.17190/AMF/1246144

Rocha, A. V., & Shaver, G. R. (2009). Advantages of a two band EVI calculated from solar and photosynthetically active radiation fluxes. *Agricultural and Forest Meteorology*, *149*(9), 1560–1563. https://doi.org/10.1016/j.agrformet.2009.03.016

Rocha, A. V., & Shaver, G. R. (2011a). Burn severity influences postfire CO2 exchange in arctic tundra. *Ecological Applications*, *21*(2), 477–489. https://doi.org/10.1890/10-0255.1

Rocha, A. V., & Shaver, G. R. (2011b). Postfire energy exchange in arctic tundra: the importance and climatic implications of burn severity. *Global Change Biology*, *17*(9), 2831–2841. https://doi.org/10.1111/j.1365-2486.2011.02441.x

Rocha, A. V., & Shaver, G. R. (2015, December 14). Anatuvuk River fire scar thaw depth measurements during the 2008 to 2014 growing season. Retrieved February 8, 2017, from http://dx.doi.org/10.6073/pasta/93121fc86e6fbcf88de4a9350609aed6

Romanovsky, V. E., Ping, C.-L., Seybold, C., & Harms, D. (2017). Toolik Soil Climate Station. Retrieved March 27, 2017, from https://www.nrcs.usda.gov/wps/portal/nrcs/detail/soils/home/?cid=NRCS142P2_053712

Schuur, E. a. G., McGuire, A. D., Schädel, C., Grosse, G., Harden, J. W., Hayes, D. J., … Vonk, J. E. (2015). Climate change and the permafrost carbon feedback. *Nature*, *520*(7546), 171–179. https://doi.org/10.1038/nature14338

Schwärzel, K., Šimůnek, J., Stoffregen, H., Wessolek, G., Genuchten, V., & Th, M. (2006). Estimation of the Unsaturated Hydraulic Conductivity of Peat Soils. *Vadose Zone Journal*, *5*(2), 628–640. https://doi.org/10.2136/vzj2005.0061

Semenova, O., Lebedeva, L., Volkova, N., Korenev, I., Forkel, M., Eberle, J., & Urban, M. (2015). Detecting immediate wildfire impact on runoff in a poorly-gauged mountainous permafrost basin. *Hydrological Sciences Journal-Journal Des Sciences Hydrologiques*, *60*(7–8), 1225–1241. https://doi.org/10.1080/02626667.2014.959960

Serbin, S. P., Singh, A., McNeil, B. E., Kingdon, C. C., & Townsend, P. A. (2014). Spectroscopic determination of leaf morphological and biochemical traits for northern temperate and boreal tree species. *Ecological Applications*, *24*(7), 1651–1669. https://doi.org/10.1890/13-2110.1

Shaver, G. R., & Rocha, A. V. (2015a, December 14). Anaktuvuk River Burn Eddy Flux Measurements, 2008 Moderate Site, North Slope Alaska. Retrieved February 8, 2017, from http://dx.doi.org/10.6073/pasta/19e3802d6738c4b30cf09188a2551b10

Shaver, G. R., & Rocha, A. V. (2015b, December 14). Anaktuvuk River Burn Eddy Flux Measurements, 2008 Severe Site, North Slope Alaska. Retrieved February 8, 2017, from http://dx.doi.org/10.6073/pasta/724bd68e01ee9a59b05cdee5cfa14bbd

Shaver, G. R., & Rocha, A. V. (2015c, December 14). Anaktuvuk River Burn Eddy Flux Measurements, 2008 Unburned Site, North Slope Alaska. Retrieved February 8, 2017, from http://dx.doi.org/10.6073/pasta/48f728d2fe75541c8f4f6827ce8dc039

Shaver, G. R., & Rocha, A. V. (2015d, December 14). Anaktuvuk River Burn Eddy Flux Measurements, 2009 Moderate Site, North Slope Alaska. Retrieved February 8, 2017, from http://dx.doi.org/10.6073/pasta/3d912564439309bdf17bc75866179312

Shaver, G. R., & Rocha, A. V. (2015e, December 14). Anaktuvuk River Burn Eddy Flux Measurements, 2009 Severe Site, North Slope Alaska. Retrieved February 8, 2017, from http://dx.doi.org/10.6073/pasta/5554a6eda8082f933709e547811b85dc

Shaver, G. R., & Rocha, A. V. (2015f, December 14). Anaktuvuk River Burn Eddy Flux Measurements, 2009 Unburned Site, North Slope Alaska. Retrieved February 8, 2017, from http://dx.doi.org/10.6073/pasta/aeb3845bf779ca10f13930e1d6c90105

Shaver, G. R., & Rocha, A. V. (2015g, December 14). Anaktuvuk River Burn Eddy Flux Measurements, 2010 Moderate Site, North Slope Alaska. Retrieved February 8, 2017, from http://dx.doi.org/10.6073/pasta/abee3157f007a794edb3414e1280d71b

Shaver, G. R., & Rocha, A. V. (2015h, December 14). Anaktuvuk River Burn Eddy Flux Measurements, 2010 Severe Site, North Slope Alaska. Retrieved February 8, 2017, from http://dx.doi.org/10.6073/pasta/2330a47db633130f0972bc134e714066

Shaver, G. R., & Rocha, A. V. (2015i, December 14). Anaktuvuk River Burn Eddy Flux Measurements, 2010 Unburned Site, North Slope Alaska. Retrieved February 8, 2017, from http://dx.doi.org/10.6073/pasta/ff790bd426b262aa7d818ad7f0b2d2a4

Shaver, G. R., & Rocha, A. V. (2015j, December 14). Anaktuvuk River Burn Eddy Flux Measurements, 2011 Moderate Site, North Slope Alaska. Retrieved February 8, 2017, from http://dx.doi.org/10.6073/pasta/f7e7d023fbac22d83ad0c2e4ce191650

Shaver, G. R., & Rocha, A. V. (2015k, December 14). Anaktuvuk River Burn Eddy Flux Measurements, 2011 Severe Site, North Slope Alaska. Retrieved February 8, 2017, from http://dx.doi.org/10.6073/pasta/d384b812a12e5cfa7fdbb4032cf1abb2

Shaver, G. R., & Rocha, A. V. (2015l, December 14). Anaktuvuk River Burn Eddy Flux Measurements, 2011 Unburned Site, North Slope Alaska. Retrieved February 8, 2017, from http://dx.doi.org/10.6073/pasta/913d3843eb71f27bac3f9c97df61573e

Shaver, G. R., & Rocha, A. V. (2015m, December 14). Anaktuvuk River Burn Eddy Flux Measurements, 2012 Moderate Site, North Slope Alaska. Retrieved February 8, 2017, from http://dx.doi.org/10.6073/pasta/b5c015dbf57ba3b3ec3ee1d95a663fc5

Shaver, G. R., & Rocha, A. V. (2015n, December 14). Anaktuvuk River Burn Eddy Flux Measurements, 2012 Severe Site, North Slope Alaska. Retrieved February 8, 2017, from http://dx.doi.org/10.6073/pasta/ed412a2a1940af95ab4611212200a5c5

Shaver, G. R., & Rocha, A. V. (2015o, December 14). Anaktuvuk River Burn Eddy Flux Measurements, 2012 Unburned Site, North Slope Alaska. Retrieved February 8, 2017, from http://dx.doi.org/10.6073/pasta/67188afe29827f8b3c0277753b2a956a

Sherwood, J. H., Kettridge, N., Thompson, D. K., Morris, P. J., Silins, U., & Waddington, J. M. (2013). Effect of drainage and wildfire on peat hydrophysical properties. *Hydrological Processes*, *27*(13), 1866–1874. https://doi.org/10.1002/hyp.9820

da Silva, F. F., Wallach, R., & Chen, Y. (1993). Hydraulic properties of sphagnum peat moss and tuff (scoria) and their potential effects on water availability. *Plant and Soil*, *154*(1), 119–126. https://doi.org/10.1007/BF00011080

Smith, S. L., Riseborough, D. W., & Bonnaventure, P. P. (2015). Eighteen Year Record of Forest Fire Effects on Ground Thermal Regimes and Permafrost in the Central Mackenzie Valley, NWT, Canada. *Permafrost and Periglacial Processes*, *26*(4), 289–303. https://doi.org/10.1002/ppp.1849

Tarnawski, V. R., & Wagner, B. (1993). Modeling the thermal conductivity of frozen soils. *Cold Regions Science and Technology*, *22*(1), 19–31. https://doi.org/10.1016/0165-232X(93)90043-8

The Inkscape Team. (2015). Inkscape (Version 0.91). Retrieved from https://inkscape.org/en/

Thompson, D. K., & Waddington, J. M. (2013). Peat properties and water retention in boreal forested peatlands subject to wildfire. *Water Resources Research*, *49*(6), 3651–3658. https://doi.org/10.1002/wrcr.20278

Thompson, D. K., Benscoter, B. W., & Waddington, J. M. (2014). Water balance of a burned and unburned forested boreal peatland. *Hydrological Processes*, *28*(24), 5954–5964. https://doi.org/10.1002/hyp.10074

Treat, C. C., Wisser, D., Marchenko, S., & Frolking, S. (2013). Modelling the effects of climate change and disturbance on permafrost stability in northern organic soils. *Mires and Peat*, *12*, 2.

Van Genuchten, M. T. (1980). A closed-form equation for predicting the hydraulic conductivity of unsaturated soils. *Soil Science Society of America Journal*, *44*(5), 892. https://doi.org/10.2136/sssaj1980.03615995004400050002x

Voss, C. I. (2011a). Editor's message: Groundwater modeling fantasies —part 1, adrift in the details. *Hydrogeology Journal*, *19*(7), 1281–1284. https://doi.org/10.1007/s10040-011-0789-z

Voss, C. I. (2011b). Editor's message: Groundwater modeling fantasies—part 2, down to earth. *Hydrogeology Journal*, *19*(8), 1455–1458. https://doi.org/10.1007/s10040-011-0790-6

Voss, C. I., & Provost, A. M. (2010). *SUTRA: A Model for Saturated-Unsaturated Variable-Density Ground-Water Flow with Solute or Energy Transport* (Water Resources Investigations Report No. 02–4231). Reston VA: U.S. Geological Survey.

Walter, M. T., Brooks, E. S., McCool, D. K., King, L. G., Molnau, M., & Boll, J. (2005). Process-based snowmelt modeling: does it require more input data than temperature-index modeling? *Journal of Hydrology*, *300*(1), 65–75. https://doi.org/10.1016/j.jhydrol.2004.05.002

Walvoord, M. A., & Kurylyk, B. L. (2016). Hydrologic Impacts of Thawing Permafrost-A Review. *Vadose Zone Journal*, *15*(6). https://doi.org/10.2136/vzj2016.01.0010

Walvoord, M. A., Voss, C. I., & Wellman, T. P. (2012). Influence of permafrost distribution on groundwater flow in the context of climate-driven permafrost thaw: Example from Yukon Flats Basin, Alaska, United States. *Water Resources Research*, *48*(7), W07524. https://doi.org/10.1029/2011WR011595

Watanabe, K., & Flury, M. (2008). Capillary bundle model of hydraulic conductivity for frozen soil. *Water Resources Research*, *44*(12). https://doi.org/10.1029/2008WR007012

Wellman, T. P., Voss, C. I., & Walvoord, M. A. (2013). Impacts of climate, lake size, and supra- and sub-permafrost groundwater flow on lake-talik evolution, Yukon Flats, Alaska (USA). *Hydrogeology Journal*, *21*(1), 281–298. https://doi.org/10.1007/s10040-012-0941-4

Wickham, H. (2009). *ggplot2: Elegant Graphics for Data Analysis*. Springer-Verlag New York. Retrieved from http://ggplot2.org

Wood, S. N. (2003). Thin-plate regression splines. *Journal of the Royal Statistical Society (B)*, *65*(1), 95–114.

Wood, S. N. (2011). Fast stable restricted maximum likelihood and marginal likelihood estimation of semiparametric generalized linear models. *Journal of the Royal Statistical Society (B)*, *73*(1), 3–36.

Wood, S. N. (2017). Generalized Additive Models: An Introduction with R (2nd edition). Chapman and Hall/CRC.

Wrona, F. J., Johansson, M., Culp, J. M., Jenkins, A., Mård, J., Myers-Smith, I. H., … Wookey, P. A. (2016). Transitions in Arctic ecosystems: Ecological implications of a changing hydrological regime. *Journal of Geophysical Research: Biogeosciences*, *121*(3), 2015JG003133. https://doi.org/10.1002/2015JG003133

Yi, S., McGuire, A. D., Harden, J., Kasischke, E. S., Manies, K., Hinzman, L., … Kim, Y. (2009). Interactions between soil thermal and hydrological dynamics in the response of Alaska ecosystems to fire disturbance. *Journal of Geophysical Research-Biogeosciences*, *114*, G02015. https://doi.org/10.1029/2008JG000841

Yoshikawa, K., Bolton, W. R., Romanovsky, V. E., Fukuda, M., & Hinzman, L. D. (2002). Impacts of wildfire on the permafrost in the boreal forests of Interior Alaska. *Journal of Geophysical Research: Atmospheres*, *107*(D1), 8148. https://doi.org/10.1029/2001JD000438

Zambrano-Bigiarini, M. (2014). hydroGOF: Goodness-of-fit functions for comparison of simulated and observed hydrological time series (Version 0.3-8). Retrieved from https://CRAN.R-project.org/package=hydroGOF

Zhang, Y., Chen, W., & Cihlar, J. (2003). A process-based model for quantifying the impact of climate change on permafrost thermal regimes. *Journal of Geophysical Research: Atmospheres*, *108*(D22), 4695. https://doi.org/10.1029/2002JD003354

Zhang, Y., Carey, S. K., Quinton, W. L., Janowicz, J. R., Pomeroy, J. W., & Flerchinger, G. N. (2010). Comparison of algorithms and parameterisations for infiltration into organic-covered permafrost soils. *Hydrology and Earth System Sciences*, *14*(5), 729–750. https://doi.org/10.5194/hess-14-729-2010

Zhang, Y., Wolfe, S. A., Morse, P. D., Olthof, I., & Fraser, R. H. (2015). Spatiotemporal impacts of wildfire and climate warming on permafrost across a subarctic region, Canada. *Journal of Geophysical Research-Earth Surface*, *120*(11), 2338–2356. https://doi.org/10.1002/2015JF003679

Zhuang, Q., McGuire, A. D., O'Neill, K. P., Harden, J. W., Romanovsky, V. E., & Yarie, J. (2002). Modeling soil thermal and carbon dynamics of a fire chronosequence in interior Alaska. *Journal of Geophysical Research-Atmospheres*, *108*(D1), 8147. https://doi.org/10.1029/2001JD001244

Zipper, S. C., Dallemagne, T., Gleeson, T., Boerman, T. C., & Hartmann, A. (2018). Groundwater pumping impacts on real stream networks: Testing the performance of simple management tools. *Water Resources Research*. https://doi.org/10.1029/2018WR022707

Zipper, S. C., & Loheide, S. P. (2014). Using evapotranspiration to assess drought sensitivity on a subfield scale with HRMET, a high resolution surface energy balance model. *Agricultural and Forest Meteorology*, *197*, 91–102. https://doi.org/10.1016/j.agrformet.2014.06.009

Zipper, S. C., Schatz, J., Singh, A., Kucharik, C. J., Townsend, P. A., & Loheide, S. P. (2016). Urban heat island impacts on plant phenology: intra-urban variability and response to land cover. *Environmental Research Letters*, *11*(5), 054023. https://doi.org/10.1088/1748-9326/11/5/054023

Zipper, S. C., Schatz, J., Kucharik, C. J., & Loheide, S. P. (2017). Urban heat island-induced increases in evapotranspirative demand. *Geophysical Research Letters*, *44*(2), 2016GL072190. https://doi.org/10.1002/2016GL072190

Tables

Table 1. Numerical model parameters and discretization.

Parameter	**Value**	**Source/Notes**
Discretization		
Width (x dimension)	1D: 5 m 2D: 200 m	200 m is typical watershed half-width for Anaktuvuk River Fire region
Height (y dimension)	1D: 20 m 2D: 25 m to 20 m	Model height based on thermal bottom boundary condition (Section 2.2.2)
Slope	1D: 0% 2D: 2.5%	Rocha & Shaver (2011b)
Model Discretization (x)	5 m	
Model Discretization (y)	0.03 m (top) to 2.0 m (bottom)	
Number of Nodes/Elements	1D: 453/300 2D: 4961/4800	
Model Duration	6935 days	19 years (1998-2016), ignoring leap years

Model Timestep	1 day	
Thermal Properties		
***Organic soil solid thermal conductivity**	**0.25 to 0.69 W m^{-2} °C^{-1}**	Literature values for peat (Jafarov et al., 2013; Kurylyk et al., 2016; McKenzie et al., 2007; Treat et al., 2013)
***Mineral soil solid thermal conductivity**	**1.40 to 1.84 W m^{-2} °C^{-1}**	Mean value from Kurylyk et al. (2016) (1.62 W m^{-2} K^{-1}) +/- half of range of organic soil thermal conductivity
Organic soil solid specific heat	1920 J kg^{-1}	McKenzie et al. (2007)
Mineral soil solid specific heat	870 J kg^{-1}	Campbell & Norman (2000)
Liquid water thermal conductivity	0.6 W m^{-2} °C^{-1}	McKenzie & Voss (2013)
Liquid water specific heat	4182 J kg^{-1}	McKenzie & Voss (2013)
Ice thermal conductivity	2.13 W m^{-2} °C^{-1}	McKenzie & Voss (2013)
Ice specific heat	2108 J kg^{-1}	McKenzie & Voss (2013)
Hydrologic Properties		
***Organic soil vertical permeability**	**10^{-15} to 10^{-10} m^2**	Literature values for peat (Jiang et al., 2015b; Naasz et al., 2005; Schwärzel et al., 2006; da Silva et al., 1993; Zhang et al., 2010)
***Mineral soil vertical permeability**	**10^{-15} to 10^{-11} m^2**	Carsel & Parrish (1988) mean for silt loam soil +/- 2 orders of magnitude
Vertical/Horizontal Permeability Ratio	0.1	
***Organic soil porosity**	**0.60 to 0.80**	Volumetric water content measurements (Rocha et al., 2008a, 2008b, 2008c; Romanovsky et al., 2017)
***Mineral soil porosity**	**0.35 to 0.55**	Carsel & Parrish (1988) mean for silt loam soil +/- 0.10
Soil Freezing Properties		
Minimum liquid saturation	0.01	McKenzie & Voss (2013)
Temperature below which minimum liquid saturation occurs	-2 °C	McKenzie & Voss (2013)
Minimum relative permeability	1 x 10^{-8}	Kurylyk et al. (2016)

* parameter varied in sensitivity analysis over range given; see Section 2.2.3

Table 2. Scenarios simulated.

Scenario	**Purpose**	**Recharge Input**	**Temperature Input**	**Organic Layer Thickness [m]**
Unburned [UB]	Model calibration	Unburned ARF site	Unburned ARF site	0.18
Moderate Burn [MB]	Model validation	Moderate burn ARF site	Moderate burn ARF site	0.12
Severe Burn [SB]	Model calibration	Severe burn ARF site	Severe burn ARF site	0.09
Severe-Recharge Change Only [SB_W]	Isolate water balance change effects	Severe burn ARF site	Unburned ARF site	0.09
Severe-Temperature Change Only [SB_E]	Isolate energy balance change effects	Unburned ARF site	Severe burn ARF site	0.09

Figures

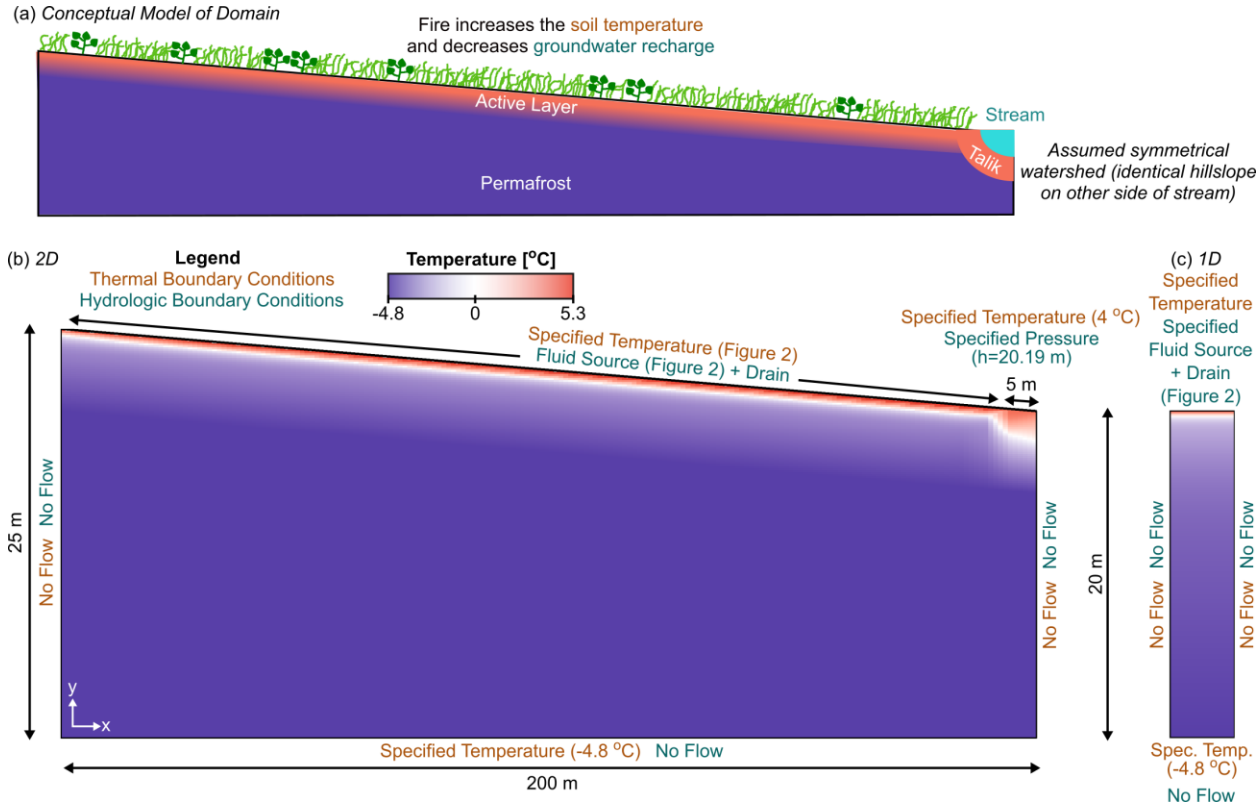

Figure 1. (a) Conceptual model of domain showing active layer underlain by permafrost with stream and talik along right edge (not to scale). Model domain for (b) 2D domain, which includes lateral groundwater flow; and (c) 1D domain, which ignores lateral groundwater flow. Colors in (b) and (c) show simulated temperature for unburned (UB) site on September 1, 2009.

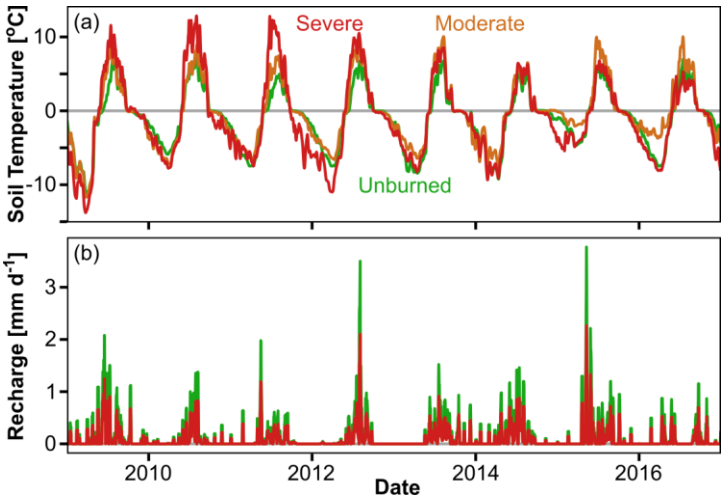

Figure 2. Upper boundary conditions applied to groundwater flow model at ARF sites. (a) Soil temperature, and (b) groundwater recharge inputs. In (b), severe and moderate inputs are the same.

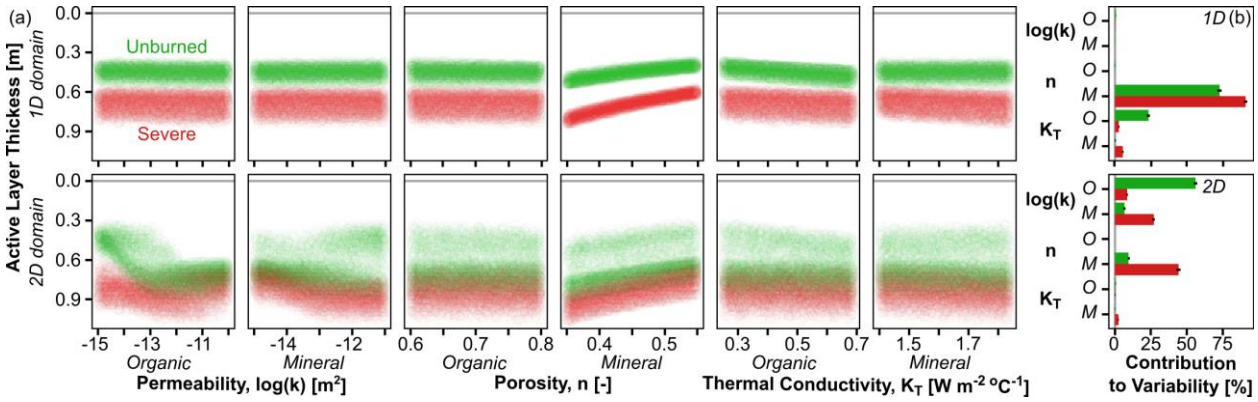

Figure 3. Sensitivity analysis showing active layer thickness response to thermal and hydrologic parameters. (a) Response of active layer thickness (averaged from all post-fire years) to variability in each parameter for (top row) 1D and (bottom) 2D domains. Each point represents one simulation from a 5000-sample sensitivity analysis. Note that the y-axis is reversed to match the orientation of Figure 1. (b) Relative contribution to observed active layer thickness variability for each parameter in (top) 1D and (bottom) 2D domains. 'O' and 'M' labels correspond to Organic and Mineral, respectively, and colors are the same as in (a). Bar length is the mean and line shows the minimum/maximum confidence interval based on 100-sample bootstrapped analysis. Combined contributions may exceed 100%.

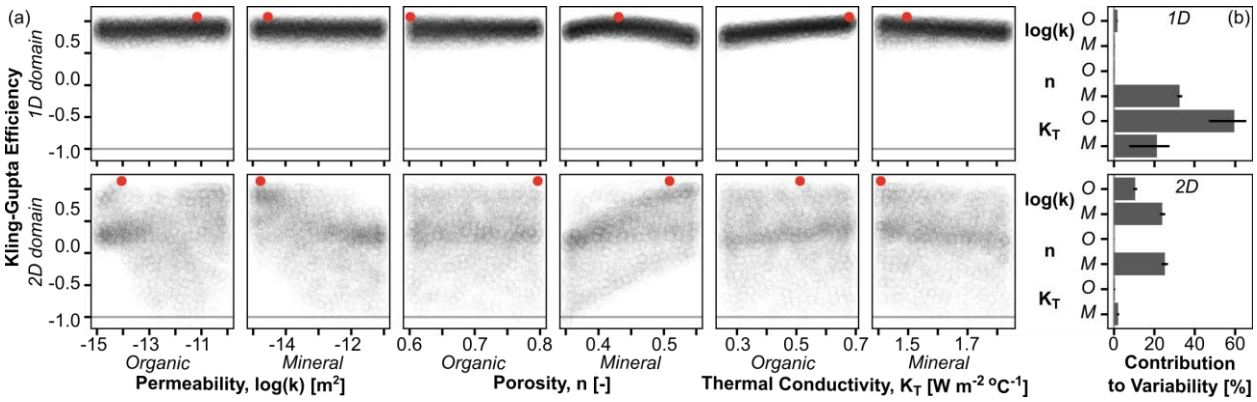

Figure 4. Sensitivity analysis showing model fit to observations as a function of thermal and hydrologic properties. (a) Response of mean Kling-Gupta Efficiency (KGE; Gupta et al., 2009) to variability in each parameter for (top row) 1D and (bottom) 2D domains. Each point represents one simulation from a 5000-sample sensitivity analysis. The red points show the calibrated parameters for 1D and 2D domains (Section 2.2.3), which are plotted in Figure 5. (b) Relative contribution to observed KGE variability for each parameter in (top) 1D and (bottom) 2D domains. 'O' and 'M' labels correspond to Organic and Mineral, respectively. Bar length is the mean and line shows the minimum/maximum confidence interval based on 100-sample bootstrapped analysis. Combined contributions may exceed 100%.

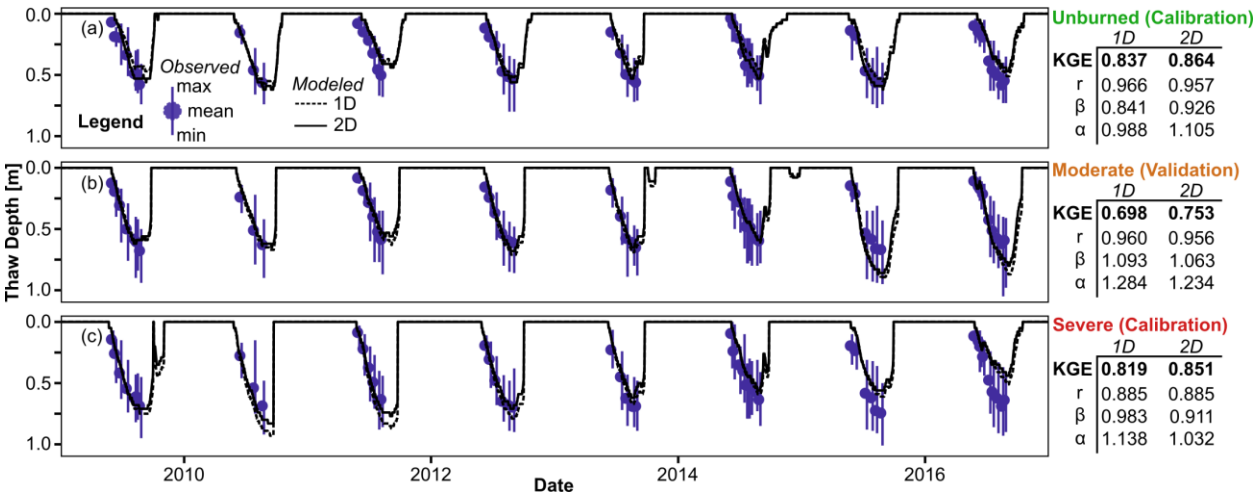

Figure 5. Model calibration and validation results for (a) unburned, (b) moderate burn, and (c) severe burn sites. Fit statistics are the overall Kling-Gupta Efficiency (KGE), as well as the decomposed KGE *r* (measure of correlation; Pearson coefficient), β (measure of bias; ratio of means of simulated to observed values), and α (measure of variability; ratio of standard deviations of simulated to observed values) parameters (Gupta et al., 2009).

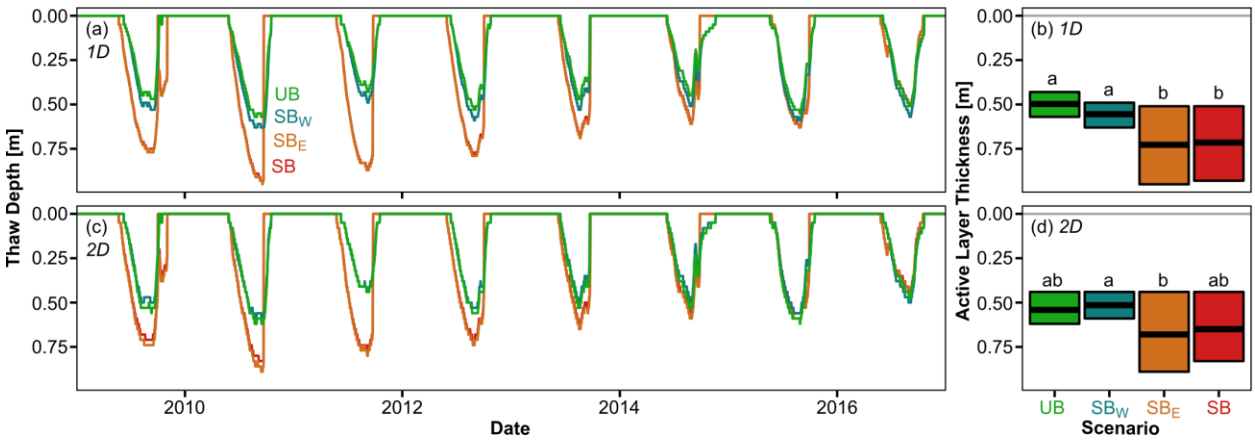

Figure 6. Comparison of daily thaw depth for different water and energy balance scenarios showing dominant effect of temperature. (a) Timeseries of thaw depth for different scenarios in 1D domain. Abbreviations correspond to Table 2. (b) Boxplot showing range and mean of active layer thickness for each scenario in 1D domain. Different letters denote significantly different means ($p<0.05$) between scenarios, as tested using the Tukey Honest Significant Differences test. (c) Thaw depth for different scenarios with 2D domain; (d) range and mean of active layer thickness for 2D domain.

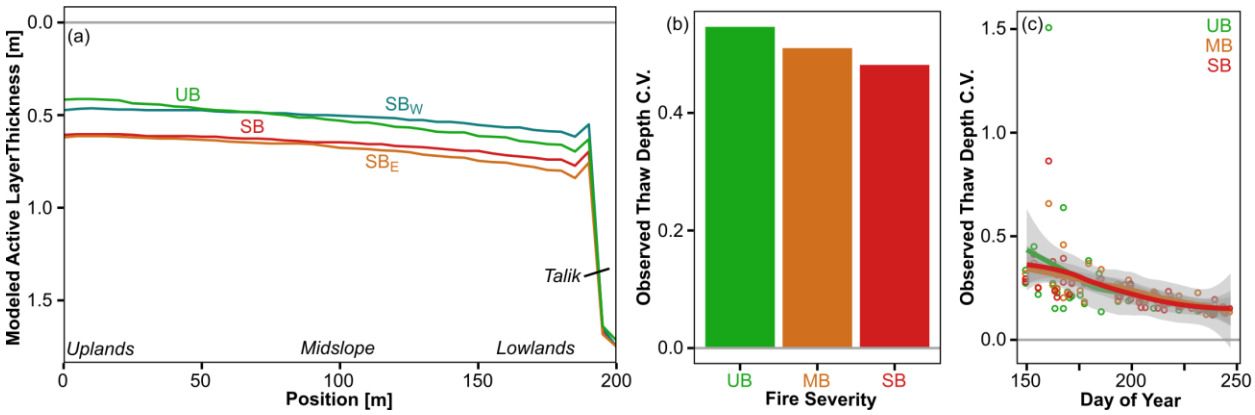

Figure 7. (a) Cross-section of modeled mean annual active layer thickness for each 2D water and energy balance scenario (colored lines). Abbreviations correspond to Table 2. Italics denote different regions referred to in the text. (b) Coefficient of variation (C.V.) for thaw depth observations grouped by site for 2009-2016. (c) C.V. of thaw depth for each site by day of year across entire 2009-2016 period. Colored lines show smoothed loess fit to all data for each site, bounded by grey confidence interval.

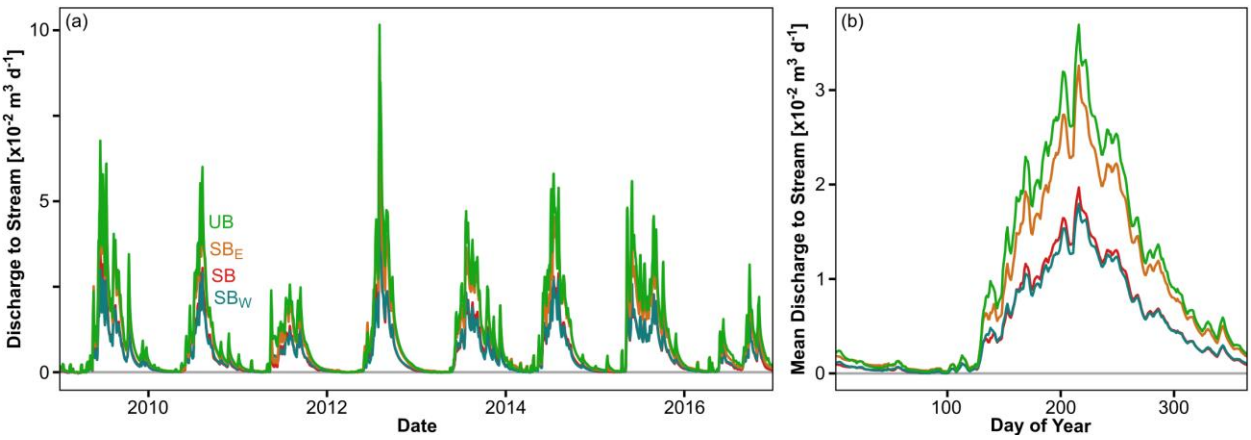

Figure 8. Discharge at specified pressure nodes representing stream for each 2D water and energy balance scenario (colored lines) for (a) entire 2009-2016 period; and (b) average for each day of year. Abbreviations correspond to Table 2.

Supplemental Information

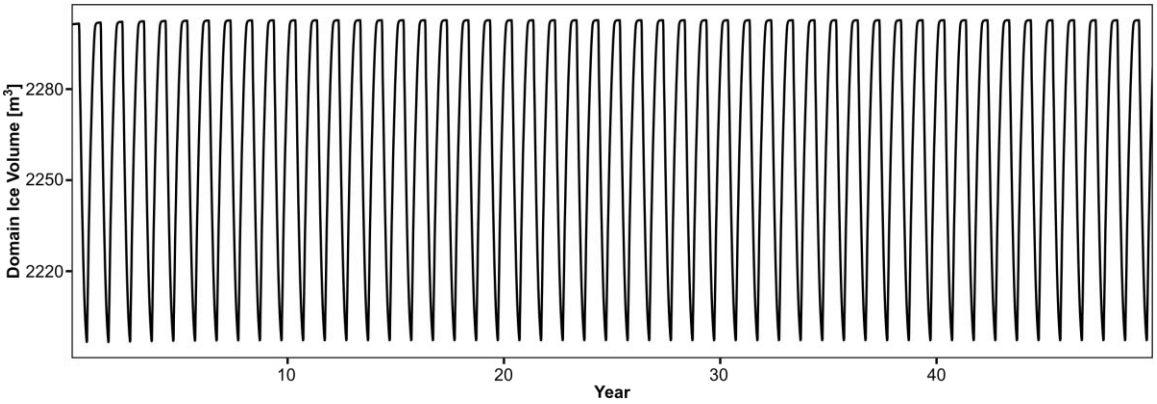

Figure S1. Total domain ice volume through time during 50 year simulation, showing that model reaches dynamic equilibrium after ~3 years (<1% change in annual range). Results in the main text have a spin-up of 10 years.

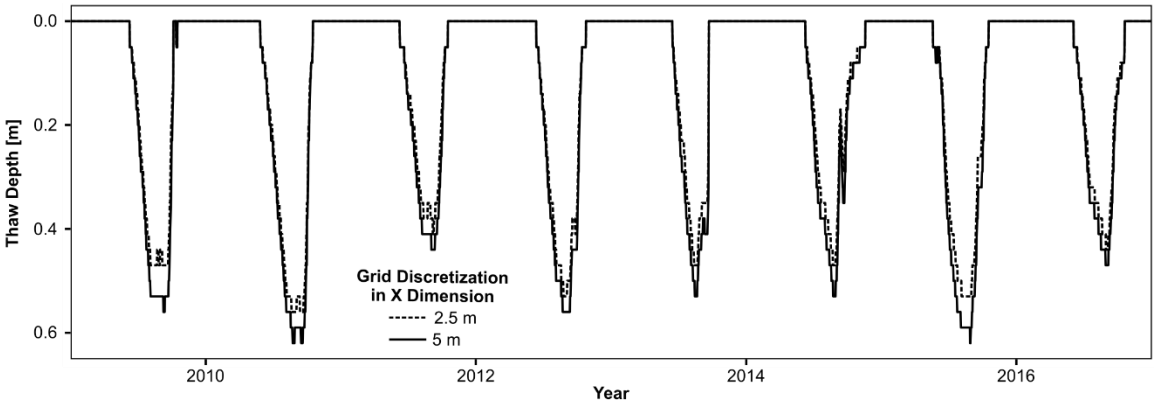

Figure S2. Annual thaw depth at the center of the model domain (x=100 m) for two different node spacings in the x dimension. Soil properties are defined using the calibrated values for the unburned site (Figure 4) and boundary conditions are recharge and soil temperature for the unburned site (Figure 2). Results in the main text use 5 m spacing.